Formation of Methanol over Copper-Zinc loaded Multi-walled Carbon Nanotubes using a Syngas feedstock

Giles Catania

Master's Thesis in Nanomaterials Science

Daily supervisors: Dr. Komal Patil, Yuang Piao MSc.
First examiner: Prof. Dr. P. E. de Jongh
Second examiner: Dr. P. Ngene

Debye Institute for Nanomaterials Science Materials Chemistry and Catalysis

Layman's Abstract

Methanol is a very important chemical, used as a building block for plastic production, fuel additives, as well as fuel. A recent shift in the energy sector to move from fossil fuels and focus on greenhouse gas capture have prompted focusing on the formation of methanol using a catalyst. Catalysts are some of the most important structures today, from being used in the catalytic converter in every vehicle to neutralize harmful gases, to the formation of margarine from liquid oils. These catalysts typically consist of two main components, a support, and the *active ingredient* which is normally a metal. In this project we used multi-walled carbon nanotubes as the supports and a mixture of copper and zinc as the active ingredient. Multi-walled carbon nanotubes are tube-shaped structures made of carbon. very similar to a paper towel roll, where each layer is made of a sheet of carbon one-atom thick! Continuing the analogy of a paper towel-roll, this has multiple layers, but only two large surfaces, the inner surface, and the outer surface. The goal of this project was to place the copper and zinc on only one of these surfaces, whilst leaving the other surface metal-free. The method we used was builds on previous work carried out within the research group, as well by other researchers. Unfortunately we did not have any luck with placing the metal on only one surface. Catalysts with metals present on all the surfaces were prepared without much difficulty. When tested to prepare methanol, these were successful, and we were able to examine how efficient these were. It turns out that catalysts which had a lower quantity of metal deposited in relation to the weight of the support, made much better use of their *active ingredient* in comparison to catalysts that had higher weights of metal. We hope that with these findings as well as our dead ends, a better method can be thought of so that the metal particles can be reliably placed where desired.

Abstract

Industrially, methanol synthesis is carried out over a $Cu/Zn/Al_2O_3$ catalyst using a feedstock consisting of $CO/CO_2/H_2$, otherwise known as syngas. Multiple publications have made use of multi-walled carbon nanotubes, otherwise known as MWCNTs as a catalyst support due to their high surface area. We attempted to produce a number of catalysts by means of incipient wetness impregnation using copper and zinc nitrates on oxidised MWCNTs. Some of these preparations underwent treatments to remove externally deposited metals, and leave only the inside deposited metal. Transmission electron microscopy showed that the selective deposition techniques were not successful, and by using a solution that will produce a 7.2 wt% Cu loading, similar results were achieved. Cu wt% loadings of 14.4+ produced large sized metal particle with large clusters found on the external nanotube surface. A significant discrepancy of 20% was observed between the intended and actual Cu wt% loading.Under methanol synthesis conditions the produced catalysts performed best at a 4 vol% CO_2 feedstock concentration. We tested the catalysts for a total of 160 hours and found that catalysts which had lower copper content had shorter lifespans in comparison to the higher copper content counterparts. The catalyst prepared with an 18 wt% Cu loading (13 wt% EDX) was found to have a 25% $CO+CO_2$ conversion into methanol which was the standout from the produced catalysts. 25% is also the upper limit for this particular reaction. Lastly, a number of new avenues of further possible investigation were identified.

Table of Contents

Title i

Layman's Abstract ii

Abstract iii

Table of contents 1

1 Introduction 2
- 1.1 Methanol synthesis catalyst development . . . 2
- 1.2 Applications of methanol . . . 3
- 1.3 Methanol formation . . . 3
  - 1.3.1 Reaction . . . 3
  - 1.3.2 Mechanism . . . 4
- 1.4 MWCNTs as supports for Methanol formation . . . 5
- 1.5 MWCNTs as supports . . . 7
  - 1.5.1 Selective deposition . . . 7
  - 1.5.2 Confinement Effect . . . 8
- 1.6 Experimental techniques . . . 8
  - 1.6.1 Cleaning and Cutting . . . 8
  - 1.6.2 Why heat-treat and oxidise? . . . 8

2 Project Aims 10

3 Experimental 11
- 3.1 Chemicals . . . 11
- 3.2 Material preparation . . . 11
  - 3.2.1 Oxidation and purification through refluxing. . . . 11
- 3.3 Catalyst preparation . . . 11
  - 3.3.1 Preparation of Cu/Zn solutions . . . 11
  - 3.3.2 Incipient wetness impregnation . . . 11
  - 3.3.3 Selective deposition . . . 12
  - 3.3.4 Sequential deposition . . . 12
  - 3.3.5 Heat treatment . . . 13
- 3.4 Characterization . . . 13
  - 3.4.1 Mass titration . . . 13
  - 3.4.2 N_2 Physisorption . . . 14
  - 3.4.3 Thermogravimetric analysis coupled mass-spectrometry . . . 14
  - 3.4.4 X-Ray Diffraction . . . 15
  - 3.4.5 Transmission Electron Microscopy . . . 15
  - 3.4.6 Particle size analysis . . . 15
  - 3.4.7 Temperature Programmed Reduction . . . 16
  - 3.4.8 Prepared Supports . . . 16
- 3.5 Catalytic testing . . . 17

4 Results and Discussion 18
- 4.1 Support point of zero charge . . . 18

4.2 Material porosity and surface area 19
4.3 Support thermal stability 20
4.4 Metal composition 23
4.5 TEM 24
4.6 Elemental analysis 28
4.7 Particle size analysis 29
4.8 Catalyst behaviour under reducing conditions 30
4.9 Catalytic activity 31

5 Conclusion **36**

6 Outlook **36**

7 Acknowledgements **37**

8 References **43**

9 Appendix **44**

1 Introduction

1.1 Methanol synthesis catalyst development

Syngas production is a very efficient technique which converts methane and coal, two fuels which have a very serious environmental impact, into feedstocks with numerous applications.[1] Syngas typically consists of carbon monoxide and hydrogen as the major mole fractions (>25%), water and carbon dioxide as the minor mole fractions (≤20%), and trace quantities of other gases such as hydrogen sulfide, argon, nitrogen, and methane.[2] Introducing a catalyst in this system, allows for the hydrogen to react with the carbon mono- and dioxides to form methanol, and in the presence of an acid, dimethyl ether.[3–6]

Some of the earliest research done on this process was carried out by Sabatier and Senderens in 1905.[8] They focused on methanol decomposition with the assumption that this can be utilized for synthesis under alternative conditions. Copper stood out as a good catalyst for decomposition, and to a lesser extent, methanol formation. The next major step came in 1926 with the research carried out by Mitttasch and Pier at BASF who pioneered the use of syngas as a feedstock for this reaction.[9] Their process involved using Cr_2O_3-ZnO as a catalyst, a temperature range of 300 - 400 °C, and a pressure of around 300 bar. The reaction yields were far from ideal and conversion was very low, so to overcome this the industrial reactor was set up in such a way to cycle the unreacted products back through the system repetitively, to push the conversion higher (Figure 1).[7] This will be further explained in section ??.

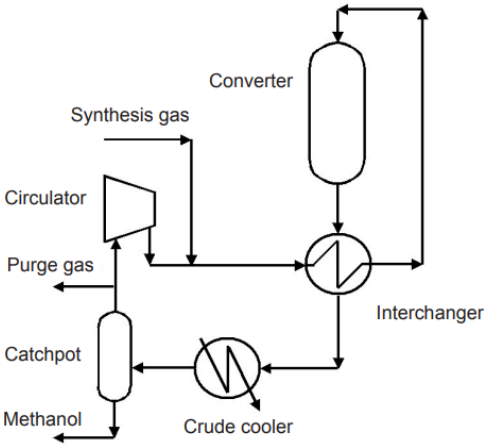

Figure 1: Layout of a pressurized methanol synthesis loop[7]

They made use of such harsh conditions, especially in terms of pressure, to increase the conversion into methanol. The next advancement came in the form of a patent made in 1947 by Błasiak, where the formation of a catalyst containing copper, zinc, and alumina (CZA) by co-precipitation is detailed.[10] The patent claimed that this catalyst is highly active and time has proven this to be absolutely true! By the 1960s, the feedstock had shifted to natural gas reforming, so the catalyst had to resist poisoning by sulfur which is present in natural gas.[7] At this point in time, natural gas was a very cheap feedstock and with oil exploration flourishing, research shifted focus from syngas to natural gas.[11,12]

The next development was made by research carried out at Imperial Chemical Industries (ICI), and patented by Davies et al.[13] They made use of a copper, zinc, and chromium catalyst at pressures in the range of 30 - 120 bar, and temperatures of 200 - 300 °C which are far milder than what was being used in the decades prior. The combination of lower pressures and temperatures greatly favoured methanol selectivity. Parallel research carried out at ICI also pioneered steam reforming, which was incorporated into the input stream for methanol synthesis. Gallagher et al. working at ICI found that catalysts containing oxides of copper, zinc, and an element from Groups II to IV, resulted in very good activity.[14] In 1966, this catalyst was installed in a reactor with a capacity of 300

metric tonnes per day with an expected lifetime of approximately six months, however it proved to be such a good catalyst that after two years, it was still producing 400 metric tonnes per day. [15] This catalyst served as the foundation for modern catalyst design which is currently used.[16] Current plants are able to produce methanol at volumes well in excess of 5000 metric tonnes per day, with plans to build facilities which are able to manufacture even bigger quantities.[7] Methanol production has grown to such large scales in order to keep up with the ever-increasing demand.

1.2 Applications of methanol

The majority of the methanol produced currently is used to produce formaldehyde which can itself be rapidly polymerized to form a number of plastic products.[17,18] Two methanol molecules can be dehydrated to form dimetheyl ether (DME). Aerosol spray formulations typically require a propellant to help add pressure to the system and allow for the formulation to exit the container at a high velocity. Chlorofluorocarbons are very good for this purpose since they compress well, and they are inert and non-flammable making them very safe, however they become environmentally damaging upon photodissociation in the stratosphere.[19] DME has been found to work well as an alternative propellant in spray formulations.[20] Its high polarity allows it to solubilize products much better than alternatives and so the aerosol provides a more homogenous spray.

Due to increased climate change awareness in recent years, the use of fossil fuels as energy sources has come under scrutiny. This has prompted development in fuel blends with gasoline and methanol. These blends show good automotive performance with the upside of reducing tail pipe emissions, and they do not require any special modification to both the engine as well as existing infrastructure.[21] This can be taken a step further to where the methanol is catalytically converted into gasoline.[22] Combining this with improvements in carbon sequestration technology brings the energy sector closer to a circular economy.[23]

1.3 Methanol formation

1.3.1 Reaction

The synthesis of methanol via CO and CO_2 hydrogenation takes place simultaneously via two reactions (Equations 1 & 2 respectively).[7,24]

$$\begin{aligned} \mathrm{CO} + 2\,\mathrm{H_2} &\rightleftharpoons \mathrm{CH_3OH} \\ \Delta H_{298} &= -91 \text{ kJ mol}^{-1} \\ \Delta G_{298} &= -25.34 \text{ kJ mol}^{-1} \end{aligned} \tag{1}$$

$$\begin{aligned} \mathrm{CO_2} + 3\,\mathrm{H_2} &\rightleftharpoons \mathrm{CH_3OH} + \mathrm{H_2O} \\ \Delta H_{298} &= -49.5 \text{ kJ mol}^{-1} \\ \Delta G_{298} &= -3.30 \text{ kJ mol}^{-1} \end{aligned} \tag{2}$$

Both reactions are thermodynamically favourable at low temperatures, however their single-pass conversion is rater low at 15 to 25%.[7] It is due to this that industrially the residual gases are recycled through the system a number of times (Figure 1).

$$\begin{aligned} \mathrm{CO} + \mathrm{H_2O} &\longrightarrow \mathrm{H_2} + \mathrm{CO_2} \\ \Delta H_{298} &= -41.2 \text{ kJ mol}^{-1} \\ \Delta G_{298} &= -28.6 \text{ kJ mol}^{-1} \end{aligned} \tag{3}$$

The water gas-shift reaction (Equation 3), is occuring in parallel with the the methanol formation (Equations 1 & 2), and this serves to consume the water byproduct formed and reform CO_2.[25] This produces CO_2, in turn driving the reaction further forward by increasing the reactant concentration and allowing for more methanol to be formed before reaching equilibrium. The reaction for the methanol formation is rather straightforward, however this starts becoming somewhat more complex if you take into consideration that the reaction occurs over a bi-metallic catalyst with the formation of intermediates and undesirable side-products.[26]

1.3.2 Mechanism

The complete reaction method is very extensive and the subject of much debate which falls outside the scope of this project.[26,27] Additionally since this project is at a small scale, the intermediates are formed in too small volumes and their presence in the final product stream is not observable in analysis. The mechanism proposed by Saussey and Lavalley explains the reaction taking place where the catlayst components each play an important part [28]:

$$\underline{\textbf{ZnO}} \qquad \begin{aligned} \mathrm{OH_{(su)}} + \mathrm{CO} &\longrightarrow \mathrm{HCOOH_{(a)}} \\ \mathrm{HCOO_{(a)}} + 2\,\mathrm{H_{(a)}} &\longrightarrow \mathrm{CH_3O_{(a)}} + \mathrm{O_{(su)}} \end{aligned} \tag{4}$$

$$\underline{\textbf{Cu}} \qquad \mathrm{CO_2} + 3\,\mathrm{H_2} \longrightarrow \mathrm{CH_3OH} + \mathrm{H_2O} \tag{5}$$

$$\underline{\textbf{ZnO}} \quad \mathrm{CH_3O_{(a)}} + \mathrm{H_2O} \longrightarrow \mathrm{CH_3OH} + \mathrm{OH_{(su)}} \tag{6}$$

With a CO feed, product formation is thought to occur through the reaction depicted in equation 1, but with the introduction of CO_2, a formate intermediate is produced and rapidly consumed (Equation 4).[29] This formate is assumed to cover the majority of the surface of the catalyst, and CO_2 acts as the major carbon source for the methanol formation (Equation 5).

---

su Surface bound
a Adsorbed

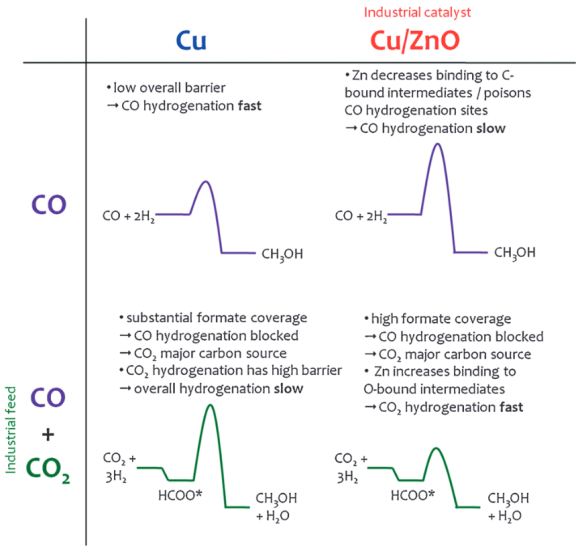

Figure 2: A comparison of the different reaction mechanisms taking place for CO, $CO+CO_2$ feedstock on Cu or Cu/ Zn catalyst. [29]

The rate of methanol production is expected to be high due to rapid CO_2 hydrogenation, as well as better thermodynamics thanks to the ZnO allowing for better binding to O-bound intermediates (Figure 2). ZnO aids in the conversion and elimination of this formate, which would otherwise temporarily poison the catalyst (Equation 6).

1.4 MWCNTs as supports for Methanol formation

As a catalyst support, carbon can take many shapes, such as amorphous activated carbon, solid tube carbon nanofibres and, hollow cylindrical tubes with single or multiple walls (CNTs and MWCNTs).[30] Generally, all carbon supports have surface areas at a minimum of 150 m^2g^{-1}. Multi-walled carbon nanotubes (MWCNTs) are hollow cylindrical structures with a multilaminate walls composed of graphene sheets (Figure 3).[31] The average inner MWCNT diameter ranges from 3 to 30 nm, and they can have a length of up to a few cm. The tube ends are capped with fullerene spheres, making the inner cavity not immediately accessible, and requires some preparatory work in order to use these as catalyst supports.[32] Due to their inner cavity, MWCNTs are not very dense, with a porosity hovering in the range of 0.7 to 1 mLg^{-1}. They are low weight, non-metallic, and chemically inert, allowing for facile characterization following metal deposition. The metal species can be clearly seen via TEM, and the phase can be determined via XRD since the peaks for the MWCNTs do not overlap transition metal peaks.[33]

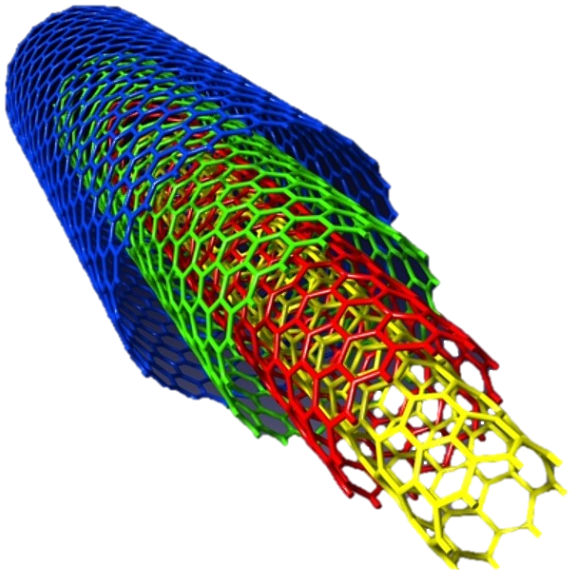

Figure 3: Structure of MWCNTs[34]

CNFs and CNTs (single- and multi-walled), have been extensively studied for the synthesis of methanol, higher alcohols, and hydroformylation, using a syngas feedstock.[35–37] Wang et al., reported that by confining copper nanoparticles within nanotubes they were able to hydrogenate methyl acetate.[38] Their findings detailed how the confinement effect played an important role in the reaction, and that during heat-treatment in pure Ar, Cu-nitrates were reduced to metallic Cu in a process described as auto-reduction. This auto-reduction property of the inner surface was also observed by Chen et al. in the preparation of Fe/MWCNT systems.[39] Fe_2O_3 deposited within the inner concave surface of MWCNTs were observed to reduce at a lower temperature in He TPR compared to their externally deposited counterparts.

Table 1: Summary of some of the most prominent publications which make use of a MWCNT/CNT support for methanol formation

Catalyst		**Mass**	**Temp.**	**Gas composition (%)**				**Pressure**	**Ref.**
Metal	**Support**	**(g)**	**(°C)**	**CO_2**	**CO**	**H_2**	**Ar/ N_2/ He**	**(bar)**	
Cu/Zn/Al/Zr	CNTs	uns.	230	5	31	64	0	40	[40]
Cu/Zn/Al_2O_3	CNTs	0.5	180-290	5	30	62	3	20-50	[35]
Cu/Zn/Al	CNTs	0.5	220	5	30	62	3	50	[41]
Mo/K	MWCNTs	2.0	290-340	0	30	60	10	41-96	[42]
Zn/ZrO_2	N-doped CNTs	1.0	450	0	35	65	0	45	[43]
Cu/ZnO	CNTs	0.05	220	4	10	72	14	80	[44]

Concentrating specifically on the hydrogenation of syngas or carbon dioxide to form methanol, we can find that this reaction has been performed by multiple groups, all using slightly different parameters and supports (Table 1). A detail not found in these projects is that they do not include any specific information or comments with regards to the position of the metal particle in the context of the multiple surfaces present in the MWCNTs. As was discussed by Miners et al. the inner and outer surfaces of the MWCNTs carry different properties, and these have a direct effect on catalysis.[32] This project aims to address that gap.

1.5 MWCNTs as supports

1.5.1 Selective deposition

The idea of selectively depositing metals onto a specific MWCNT or CNT surface, is not novel, with multiple established methods having been reported.[38,45–50] However, with regards to deposition of Cu/Zn selectively inside MWCNTs for the hydrogenation of syngas, literature is surprisingly sparse. These methods can be divided into three main approaches:

i **Sonication assisted deposition**

Sustained agitation of the metal-containing solution with the support allows for the entry and binding of the dissolved metal onto the concave MWCNT surface.[38] For this technique, a wet-impregnation method is used since sonication requires a dense medium to properly transmit the high frequency waves.[46] A slurry is made containing the support, and the solvent, in which the desired wt% loading is dissolved. After stirring for a prolonged period of approximately 12 hours, the mixture is sonicated to ensure complete permeation of the metal into the MWCNT pores. [47] This is then heat-treated to convert the metal salt into its oxidized state and firmly anchor it to the support.

ii **Selective washing**

Careful choice of the solvent in which the metals are dissolved is essential, in order to then choose an accompanying washing liquid which is immiscible with, and less viscous that the solvent.[48] Following incipient wetness impregnation utilizing an aqueous metal solution, the supports were suspended in an organic liquid and these removed any metal deposited on the outer layer. The support is then separated from the bulk of the liquid by filtration, and heat-treatment removes the aqueous solvent as well as any excess washing solvent. If the desired location for the metal particles is on the outside of the material, the pores are blocked through incipient wetness impregnation using an organic liquid, and then the aqueous solution is introduced to deposit particles onto the surface.[49] The last step is to heat-reat in order to remove all the liquid and anions.

iii **Controlled filling and protection using organic solvent.**

The main disadvantage of using a washing solvent which is immiscible to the 'loading' solvent is that the target metal to be removed, might be insoluble in the washing solvent. To techniques described by Capobianchi bypassess this limitation through a number of clever steps (Figure 6).[50] After depositing the metal via incipient wetness impregnation, the solvent is removed by freeze drying thereby preserving the particle distribution as it is in solution. The pores are then blocked using an organic liquid in which the metal salts are insoluble. The aqueous solvent is then to wash the exterior surface of the MWCNTs since this is very effective at dissolving the metal salts. Lastly, the loaded supports are calcined.

Due to the copper and zinc nitrate's limited solubility in organic solvents, method iii will be used in this project. This will be amended to fit the scope of this project, and instead of freeze-drying, the inital solvent removal will be carried out by heating at low temperatures under vacuum.

1.5.2 Confinement Effect

Encapsulated metals are thought to exhibit lower reduction temperatures due to the shifting in the π electron density of the graphene form the concave to the convex surface.[47] This also results in a difference in the electronic properties between the inner and outer MWCNT surfaces. Experimentally, a discrepancy should be expected in catalysis when the metal is present exclusively on either surface. One expected limitation is that the particle size within the nanotube is limited by the pore diameter, whilst a metal cluster present on the convex surface has no growth limitations.

1.6 Experimental techniques

1.6.1 Cleaning and Cutting

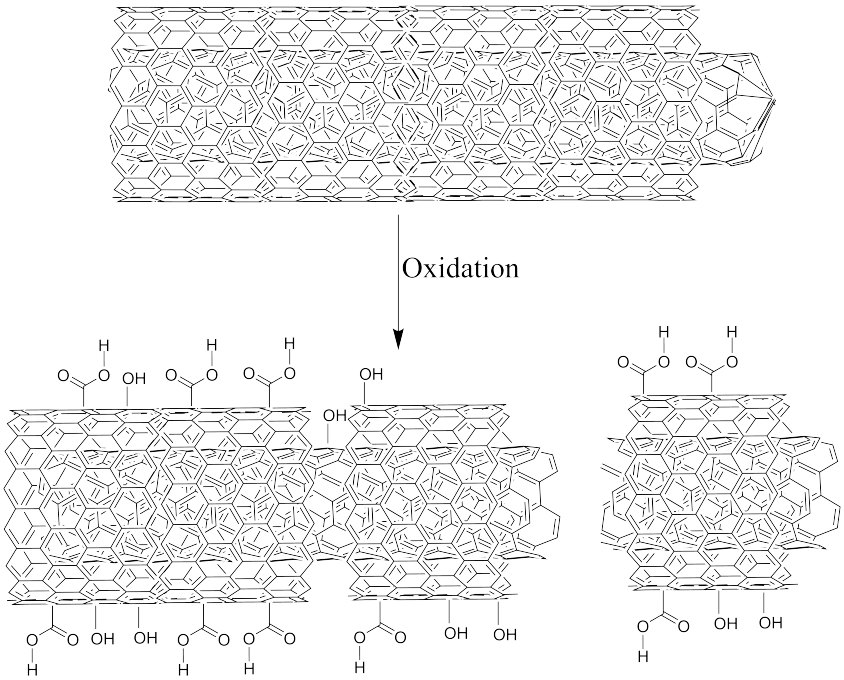

Figure 4: MWCNT activation by refluxing

The first step prior to any loading techniques carried out onto the multi-walled carbon nanotubes involved nitric acid reflux. [51] The reflux step serves a number of purposes: it opens up the ends of the nanotubes; cutting up the mwcnts to form smaller segments; and slightly oxidizing and acidify the mwcnts (Figure 4).[52] Traces of the catalyst used in MWCNT manufacturing trapped between the multi-wall layers are also removed in this step.[30] Uncapping and cutting the mwcnts increases the surface area of the structures and allows for them to take in liquid (Figure 5).[53] The surface groups produced allow for better wettability and metal particle anchoring, both of which crucial during incipient wetness impregnation.[54]

1.6.2 Why heat-treat and oxidise?

After metal deposition the supports are subjected to heat treatment to remove the nitrate anions and solvents used in the preparation. The thermal treatment will involve two

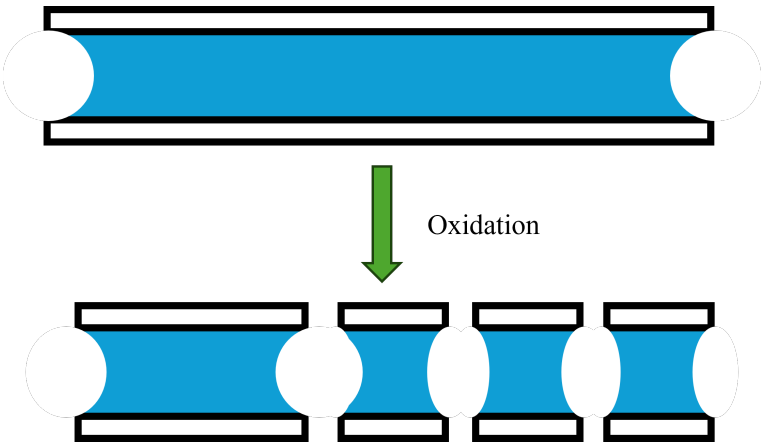

Figure 5: Segmenting of MWCNTs through the process of oxidation.

principal reactions; drying and oxidation (Equations 7 & 8).

$$\begin{aligned} \mathrm{Cu(NO_3)_2 \cdot 3\,H_2O} &\xrightarrow{\Delta} \mathrm{Cu(NO_3)_2 + 3\,H_2O} \\ \mathrm{2\,Cu(NO_3)_2} &\xrightarrow{\Delta} \mathrm{2\,CuO + 4\,NO_2 + O_2} \end{aligned} \tag{7}$$

$$\begin{aligned} \mathrm{Zn(NO_3)_2 \cdot 6\,H_2O} &\xrightarrow{\Delta} \mathrm{Zn(NO_3)_2 + 6\,H_2O} \\ \mathrm{2\,Zn(NO_3)_2} &\xrightarrow{\Delta} \mathrm{2\,ZnO + 4\,NO_2 + O_2} \end{aligned} \tag{8}$$

Drying is expected to start at approximately 30 °C and end at approximately 120 °C.[55] During this step, the water used as a solvent as well as any other solvent used in selective deposition is removed. Using a continuous gas flow helps in retaining a concentration gradient between the liquid and gaseous solvent, so drying is highly efficient even at sub-boiling temperatures. Under dry atmospheric conditions, alumina-supported metal nitrates thermally decompose at approximately 265°C for zinc nitrate, and at 246°C for copper nitrate.[55,56] Since the carbon supports are quite prone to thermal decomposition under high oxygen concentrations at temperatures in the range of 300°C, the thermal decomposition will be carried out in an inert N_2 atmosphere. The oxidation will then be carried out at a lower temperature and contact with oxygen will be minimized as much as possible.[57] Oxidation ensures all the metal present on the support is in the same phase, ensuring that XRD spectra and TPR measurements can be compared without issue.

2 Project Aims

The aim of this project is to probe the knowledge gap regarding the metal particle location on a multi-walled carbon nanotube support for the hydrogenation of CO/CO_2 to methanol. This project also serves a broader aim of gaining a better insight into the preparation and testing of heterogeneous catalysts.

The following are research questions which I aim to answer:

i Is it possible to selectively deposit a Cu/Zn nitrate solution on MWCNTs favouring one specific zone?

ii Does the concentration of the initial solution alter deposition vis-à-vis fluid uptake into the pores?

iii What effect do the different preparation techniques have on the final metal content of the catalyst?

iv How does the conversion of CO/CO_2 into methanol vary with the location of the metal in/ on the MWCNT?

3 Experimental

3.1 Chemicals

Table 2: Materials used

Name	Composition	Purity	Supplier
Baytubes C150P	C	>95%	Bayer
Nitric acid	HNO_3	65%	Normapur
Copper(II) nitrate trihydrate	$Cu(NO_3)_2 \cdot 3\,H_2O$	99%	Sigma-Aldrich
Zinc nitrate hexahydrate	$Zn(NO_3)_2 \cdot 6\,H_2O$	98%	Sigma-Aldrich

3.2 Material preparation

3.2.1 Oxidation and purification through refluxing.

The method used was adapted from a number of others, with a milder acid concentration of 35% being used to prevent the complete oxidation and decomposition of the MWCNTS.[58–60] In a 500 mL round-bottom-flask, 6 g of as-received MWCNTs were dispersed in 240 mL of 35 vol% nitric acid. A reflux condenser was attached and the mixture was stirred for a few minutes at 500 rpm to homogenize the suspension. This was then refluxed under magnetic stirring for 16 h. After that, the resulting dispersion was allowed to settle and the liquid was decanted off. The resulting solid was washed using Milli-Q®until the washing water was pH neutral. The now oxidized MWCNTs were separated from the water by vacuum filtration and transferred to a 75 mL round-bottom flask. These were dried in air 110 °C with magnetic stirring at 250 rpm to prevent the formation of large aggregates. Lastly, to ensure maximum dryness, these were dried under dynamic vacuum at 100°C for 1 hour with 250 rpm stirring. The dry, oxidized MWCNTs were stored in a glass vial at room temperature.

3.3 Catalyst preparation

3.3.1 Preparation of Cu/Zn solutions

Oxidized MWCNTs were loaded with a solution containing copper and zinc nitrates at a molar ratio of 2.64 to 1 respectively. The concentration was varied to achieve the desired wt% loading. Solution preparation required achieving a balance between a number of parameters, all of which are interconnected. The metal nitrates were weighed in accordance to the mass of support, and then placed in the appropriate volumetric flask. This was dissolved with Milli-Q®water. To ensure consistency, for each concentration one deposition solution was prepared, and kept at a low temperature in the dark to prevent evaporation or degradation. Under these conditions a solution should have a long lifetime and can be sufficiently used throughout the whole project as needed.

3.3.2 Incipient wetness impregnation

The catalysts prepared in this project were all prepared via incipient wetness impregnation. Prior to adding the support, a round-bottom flask with a rubber septum, and an angled attachment which contained a frit and a tap. The flask was emptied under

vacuum and this was weighed. The flask was then opened, the supports were added, and then dried under dynamic vacuum. The mass of the supports was then determined by comparing the mass of the empty and full flasks. Using this mass, the volume to be injected to achieve the desired weight loading was calculated. Under strong stirring and static vacuum, a third of the deposition solution is injected and the support is left to stir for a minute. during this time, the round bottom flask was also physically moved so that the stir bar makes contact with the edges and completely homogenizes the nanotubes. This was repeated twice more until all of the solution was injected. This was done to avoid any *hotspot areas* which would have received more solution than others. After the loading was complete, the mwcnts were then dried under a dynamic vacuum and transferred to a calcination tube.

3.3.3 Selective deposition

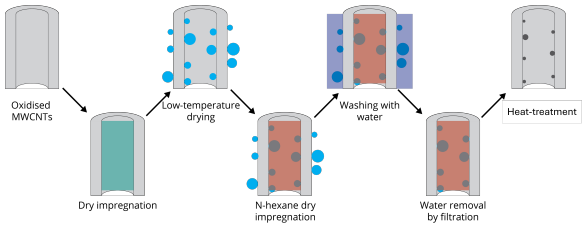

Figure 6: General procedure of selective loading

The selective loading procedure involved first loading the oxidized MWCNTs with a 95% pv solution with the desired wt% loading (Figure 6). This was then dried at 100°C under dynamic vacuum with stirring. A 95% pore volume of n-hexane was then injected to occupy the internal spaces within the MWCNTs. The supports were then removed from the round bottom flask and suspended in 25 mL of distilled water (for 1g of starter material), and gently swirled. The water was removed by vacuum filtration, and the MWCNTs were rinsed once more inside the funnel with an additional 25 mL of water. The MWCNTs were transferred to a calcination-reduction tube for heat treatment and oxidation. Selective loading on the external surface was performed by first blocking the pores with n-hexane, and then immediately injecting a 95% pv solution containing the desired Cu/Zn wt%.

3.3.4 Sequential deposition

To analyse if the position of the metal particles onto the support is dependant on the wt% concentration of the solution as well as the pore volume, sequential loading was used. Here, two different approaches were used. For the catalyst 2E14, incipient wetness impregnation of a solution of 7.2/2.8 Cu/Zn wt% was used at 95% pore volume. After the first loading, the support was dried under dynamic vacuum, and then the loading was performed once more to get a final wt% loading of 14.4/5.6. The catalyst 2E18 was prepared by using a solution of 9/3.5 wt% and loading it to 47.5% of the pore volume. After dynamic vacuum drying, the solution was loaded once more onto the support.

3.3.5 Heat treatment

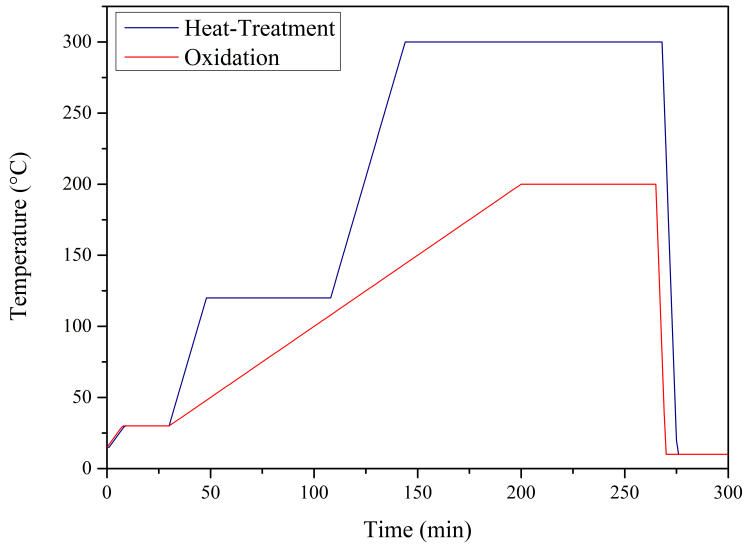

Figure 7: Temperature profile for heat-treatment and oxidation.

After loading the supports, they were all subjected to heat-treatment. This was carried out under an inert N_2 atmosphere. N_2 flow was set at 100 mL/min throughout the whole process. The temperature profile was set as shown in figure 7. This was separated into 4 segments. The catalyst was flushed with nitrogen to equilibrate the system with the new gas composition as well start drying. The next step was drying, where the system was held at 120°C for 1 hour. This was then immediately followed by oxidation which held the system at 300°C for approximately 2 hours. After heat treatment, the system was air cooled to room temperature.

To handle the materials and ensure that the metal species were all in the oxidized state, the material was oxidized under gentle conditions. The temperature profile and conditions used were adopted from previous work done within the group by Dalebout et al.[61] During the oxidation process (Figure 7), a 5/95 mLmin^{-1} O_2/N_2 gas composition was first used. This was kept until the start of the oxidation process, at which point a composition of 15/85 mLmin^{-1} O_2/N_2 was used. Thermal decomposition under oxygen rich atmospheres starts off at 200°C , so it was essential to minimize contact time with high oxygen concentrations.[57]

3.4 Characterization

3.4.1 Mass titration

To quantify which reflux treatment was the most effective at imparting acidic groups onto the mwcnts, a mass titration was used, with a method adapted from Donoeva et al.[62] This technique relies on starting with a fixed volume of a pH neutral liquid, in this case, 5mL Milli-Q® water. Stepwise, 25 mg increments of solid are added. After each addition, the suspension was stirred at 100 rpm and the pH was measured using the pH probe from a Metrohm 888 titrando apparatus. This was repeated until the isoelectric point was reached, ie. when successive pH measurements after material addition result in the same pH. At this point it can be said that the water is saturated with H_3O^+ anions and

the material is unable to donate more protons due to the acidic surface groups reaching their dissociation constant. Due to the many different surface groups that refluxing may introduce on the material, it is rather difficult to theoretically determine the isoelectric point of the oxidized supports.

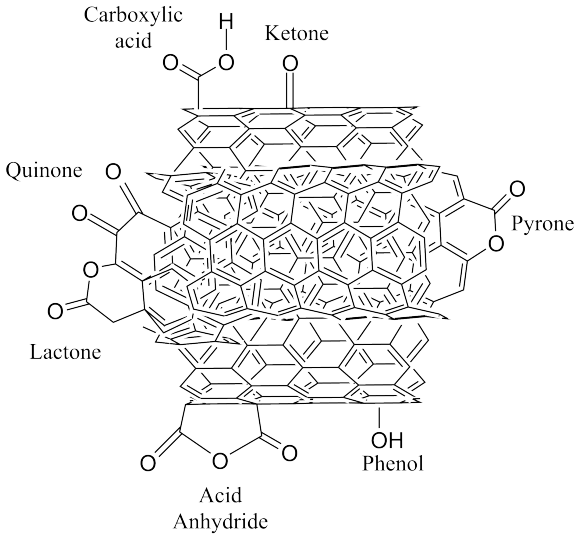

Figure 8: Surface groups as a result from oxidation. Carboxylic acids, phenols, and lactones are Brønsted acids, with the other groups being basic.[63]

3.4.2 N_2 Physisorption

Material porosity metrics were essential for incipient wetness impregnation, and after deposition, it serves as a useful tool to assess the impact of applied treatments. Characterization was carried out at -195.8°C (77 K) with a Micrometrics®TriStarII PLUS used for pore volume (pv) quantification. Following a drying step carried out under vacuum, the pore volume was measured using N_2 physisorption. For surface area determination, Brunauer-Emmett-Teller (BET) analysis was performed at $0.05 \leq p/p_0 \geq 0.25$. Where p/p_0 refers to the relative pressure. For micro- and mesoporosity quantification, t-plot analysis was carried out based on a Harkins and Jura reference isotherm. Lastly, Barrett-Joyner-Halenda (BJH) analysis was employed to estimate pore size, and the cumulative pore volume of the supports. When presenting the results, they are given at STP. The single point adsorption at the highest measured p/p_0 for a material was taken to be the cumulative pore volume. The porosity is follows the order of micro $<$ meso $<$ macro, with diameters (nm) of 0 - 1.7 $<$ 1.7 - 300 $<$ 300+ respectively.

3.4.3 Thermogravimetric analysis coupled mass-spectrometry

To conduct this measurement, a TA Instruments Discovery TGA5500 was used in conjunction with an MKS Cirrus^{TM} 3 mass spectrometer. TGA-MS served useful for a number of questions, especially early on in the project. It was used to find the thermal decomposition temperature of the metal nitrates, and hence the heat-treatment temperature was found. Moreover, it was also used to determine the stability of the supports which is of paramount importance considering that they will be used in a high temperature environment. The metal-free supports were subject to TGA in a pure Ar environment and the support containing metal nitrates were subjected to 20 vol% O_2 in Ar. The

experimental run consisted of a flushing step with 20 mLmin^{-1}N$_2$ for 30 min at 30°C. Then the gas composition was switched to either pure Ar or an O_2/Ar blend and heating was applied at a rate of 10°C/min until 800°C was reached.

3.4.4 X-Ray Diffraction

To determine the phase the deposited metal is in as well as the facets available for catalysis powder X-ray diffraction (XRD) scans were taken. A Bruker AXS®D2 Phaser (2nd generation) diffractometer was used with a fixed slit of 1 mm, and a 30 kV, 10 mA X-ray source at room temperature. The powdered material was placed in the sample holder and irradiated with CoK$\alpha_{1,2}$ radiation (λ = 1.79026 Å). Scan parameters were set with a time/step of 1s, starting at $2\theta(^\circ)$ of 10°, and ending at 90°, with an increment of 0.05°. Each scan had a duration of approximately 30 minutes, and for each measurement, 4 consecutive scans were taken to eliminate noise and enhance accuracy.

3.4.5 Transmission Electron Microscopy

In preparation for TEM imaging, the supports were suspended in ethanol and sonicated to ensure the breakup of any clumps. This suspension was then carefully dropcasted onto a carbon-coated Cu-grid (300 mesh) and dried. This grid was then placed in the holder for the FEI Talos^{TM} F200X. The sample was loaded and a vacuum was pulled in the system and the 200 kV beam was used to obtain detailed images.

Energy-dispersive X-ray (EDX) images were taken to measure the metal content present on the supports. The catalysts were dropcast over an Au-grid to eliminate any overlap between the grid material and the deposited metals.

3.4.6 Particle size analysis

Using the TEM images, the size of the particles deposited onto MWCNTs was measured. Through the use of ImageJ, the metal particles were individually sized. For each wt% loading, at least 100 particles were measured (with the exception of one catalyst which did not have enough particles across all images). The measurements were used to plot histograms and box and whisker plots (Figures 26 & 20). For the histograms, a bin size which corresponds to 4% of the x-axis is used so that the data is represented in an equivalent way without adding too much noise. The average and standard deviation are presented along with the sample size (N). The box whisker plots are constructed using the complete dataset for each catalyst, with the data maxima being represented by a $-$, the values at the 99% of the maxima with a $\times$, and the mean with a $\square$. The whisker porton represents 5 to 95% of the dataset, and the box represents 25 to 75%. The line within the box represents the median which is the absolute middle of the dataset regardless of distribution or skewness.

3.4.7 Temperature Programmed Reduction

The behaviour of the catalysts under a reducing environment was analysed using 5% H_2/Ar TPR in a Micrometrics® AutochemIII. Prior to starting the TPR, the catalyst heated to 120 °C at a rate of 10°C min^{-}1 under inert Argon flow to dry the material. After drying, the heating was switch off and cold argon was flushed through to cool it down to room temperature. The gas flow was then switched to the 5% H_2/Ar at a flow-rate of 25 cm^{3}min^{-1}. The heating was turned on at a rate of 5°C min^{-1} until it reached 500°C. The system was then allowed to cool down, after which the catalyst was collected and discarded. The results from this instrument were vital for catalytic testing since the catalyst was *in situ* reduced prior to starting testing.

3.4.8 Prepared Supports

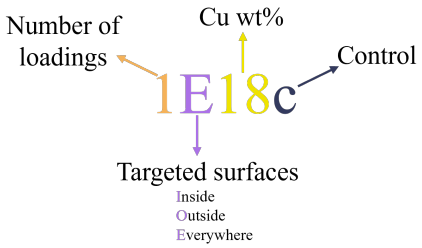

Figure 9: Catalyst naming key

Table 3 shows all the produced catalysts which were used in this procedure. The short-hand naming convention for all the catalysts produced is shown in figure 9.

Table 3: Summary of all the different treatments applied to the MWCNTs

Name	Description	Wt%	
		Cu	Zn
Mw	Pristine MWCNTs	0	0
Ox	MWCNTs refluxed with 35 vol% HNO_3 for 16 hours	0	0
1E18	Ox, loaded with a 95% pv solution	18	7
1E7	Ox, loaded with a 95% pv solution	7.2	2.8
1I18	Ox, internal loading	18	7
1I7	Ox, internal loading	7.2	2.8
1I7c	Ox, internal loading, no n-hexane used to serve as a control	7.2	2.8
1O7	Ox, external loading	7.2	2.8
2E14	Ox, loaded twice with a 7.2/2.8 wt% solution at 95% pv	14.4	5.6
2E18	Ox, loaded twice with an 9/3.5 wt% solution at 47.5% pv	18	7

3.5 Catalytic testing

Space velocity is inversely correlated with the conversion, however the turnover frequency and yield are positively correlated.[24,64] The conditions chosen must achieve a balance between this, and as a starting point, previous work carried out within the group will be referred to.[61] The stability and catalytic performance of Cu/Zn impregnated MWCNTs was investigated by subjecting them to methanol synthesis conditions for 160 hrs. This took place in an Avantium Flowrence II 16-bed reactor. Each stainless-steel reactor tube was packed with 15 - 60 mg of catalyst (sieve fraction 75 - 150 μm), and 180 mg of inert SiC (sieve fraction 212 - 425 μm), sandwiched between two protective SiC layers. A cross section of a typical reactor can be seen in figure 10. The SiC served to both minimize hot-spots and ensure sufficient gas flow in the catalytic zone, and in the upper and lower layers served to hold the lightweight support in place and prevent it from being disturbed. The tubes were placed inside the Flowrence II, and a list of the tested catalysts can be found in the appendix (Table 7). The self-made catalysts were all tested at a mass of approximately 60 and 30 mg. By halving the mass, the GHSV was effectively doubled.

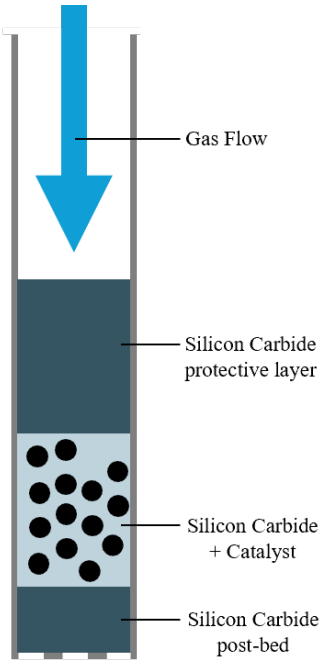

Figure 10: Loading of the Flowrence II reactors

Table 4: Individual reactor flow-rates (NmL/min)

He	**H_2**	**CO**	**CO_2**	**Total**
0.25	1.50	0.75	0	2.5
0.25	1.50	0.75	0.03	2.5
0.25	1.50	0.65	0.10	2.5
0.25	1.50	0.58	0.17	2.5

Four sequential catalytic tests were carried out, with each subsequent test increasing the CO_2 concentration. Prior to testing, the catalysts were *in situ* reduced with an H_2 rich flow at 120°C. After reduction, the system was slowly heated to 240°C, and pressurized to 40 bar. Each gas composition was ran for approximately 34 hours. Between the compositions, the system was depressurized, flushed with inert gas, and then re-pressurized with the new gas composition. The outlet gas stream from each reactor tube was analysed via online gas chromatography. This switched its source (reactor) every 15 minutes. At the end of the experiment, the end result was a time-resolved GC composition for the different conditions applied throughout the whole experiment.

4 Results and Discussion

4.1 Support point of zero charge

Mass titrations to determine the point of zero charge (PZC) for the materials yielded the plot presented in figure 11. The results show that generally, after the addition of approximately 300 mg of catalyst/ support, the PZC was reached. The exception to this is the Ox support, which reached its PZC after the addition of 100 mg. The pH at the PZC is above 7 for all the different samples, with the exception of Ox, which had a very acidic PZC pH of 3.

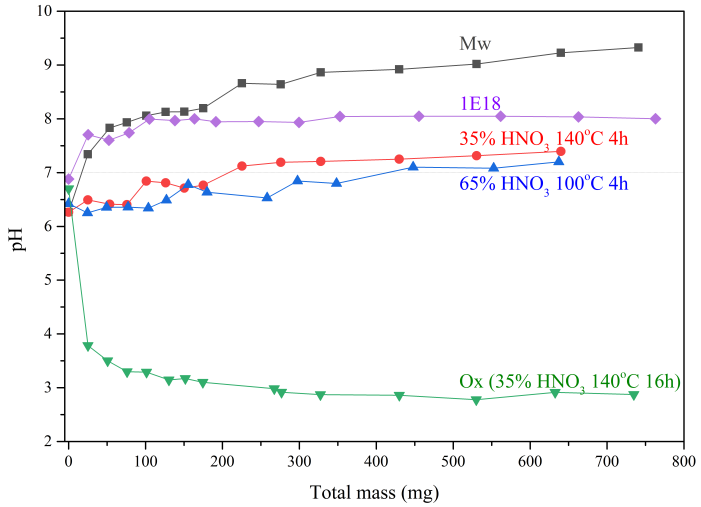

Figure 11: Mass titration of acid-oxidised MWCNTs, pristine MWCNTs, and a prepared heat-treated and oxidised catalyst in 5mL Milli-Q®water.

Mw had the most basic PZC pH of the tested supports, and this was expected since this is pristine material which did not undergo any oxidation treatments, a process by which acidic groups were added onto the surface. [52] The two supports prepared by using a 4 hr reflux period ended up with a very similar PZC pH. The supports produced by a 4 hr reflux in 35 vol% HNO_3 were not exposed to the acid for long enough for it to adequately modify the surface. On the other hand, the supports treated in 65 vol% HNO_3 for 4 hr were not properly refluxed since 100 °C is below the temperature range at which the acid boils (117 - 123 °C). The Ox supports rectified these missteps and this was refluxed in HNO_3 for 16 hr. This produced the desirable results of highly acidic oxidised-MWCNTs which were also segmented into smaller chunks (Figure 17b).

This highly acidic MWCNT support, termed Ox was used for catalyst preparation. A catalyst prepared through incipient wetness impregnation to a desired Cu wt% of 18, and then heat-treated and oxidised, was subject to mass titration. This catalyst had a PZC of pH 8, which meant that during the heat-treatment steps, the labile acidic groups present on the Ox support were lost. Although this change should not have any adverse effect on the production of methanol, it does mean that the catalyst is unsuitable for dimethyl ether production since it is thermally unstable. This is also backed up by other studies, where dimethyl production over a similar system makes use of an additional component as the source of acidity required for methanol dehydration.[6]

4.2 Material porosity and surface area

N_2 physisorption of pristine, and oxidised supports along with prepared catalysts can provide a good idea of how the supports change as the different metal loading procedures are applied to them. The isotherm shows that the bulk pore volume is present as mesopores with some desorption hysteresis.(Figure 12).

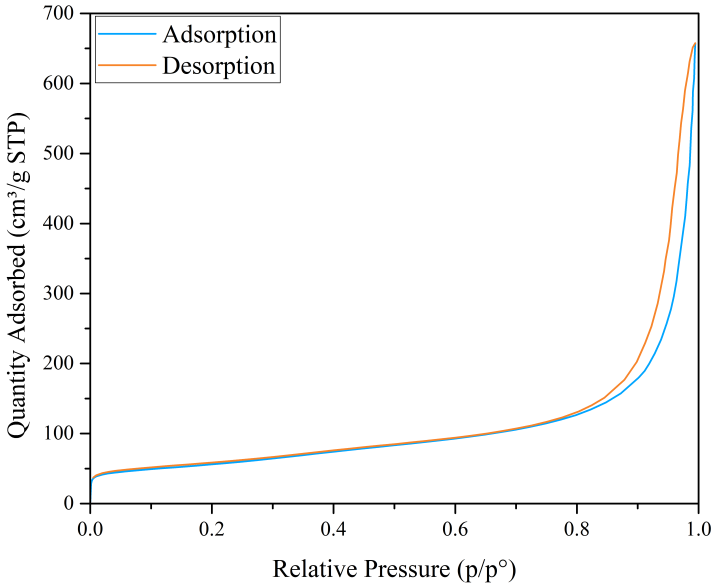

Figure 12: N_2 Physisorption isotherm at 77 K with adsorption and desorption branches for pristine MWCNTs which are a IUPAC H1 isotherm. (The rest of the supports are the same and can be found in the appendix section)

Pristine supports had the highest pore volume, with most of the porosity being present as mesopores (Table 5). The oxidation process produced an increase in the surface area of the supports, especially in mesopore area, with a decrease in the micropore area, and total volume. The supports which underwent selective deposition favouring the internal MWCNT surface, i.e. 1I18, 1I7, 1I7c, all had a higher pore area than the initial support, and a 1I7 had a pore volume equal to pristine MWCNTs.

Table 5: Pore volume and area metrics obtained through N_2 physisorption

Catalyst	**Area (m^2g^{-1})**			**Volume (cm^3g^{-1})**			
	Micropore	**Mesopore**	**Total**	**Micropore**	**Mesopore**	**Macropore**	**Total**
Mw	37.42	159.8	197.2	0.0178	0.911	0.088	1.02
Ox	16.92	209.5	226.4	0.0095	0.736	0.087	0.83
1E18	7.57	142.3	149.8	0.0033	0.695	0.024	0.72
1E7	17.68	151.3	169.0	0.0086	0.756	0.061	0.83
1I18	31.02	193.3	224.3	0.0145	0.613	0.081	0.71
1I7	7.14	234.3	241.5	0.0022	0.929	0.088	1.02
1I7c	21.86	221.7	243.6	0.0100	0.761	0.104	0.87
1O7	14.29	180.7	195.0	0.0071	0.690	0.040	0.74
2E14	28.47	133.9	162.4	0.0133	0.484	0.066	0.56
2E18	22.44	134.7	157.1	0.0106	0.459	0.057	0.53

The MWCNTs used have a pore diameter of 4 nm which falls within the range defined as mesopores in the BJH analysis, and this is well depicted in the measurements (Table 5).[65] Based off the hysteresis, porosity of MWCNTs is uniform and it can be defined as a type H1 according to the IUPAC classification (Figure 12).[66] Through the hysteresis loop, we can also deduce that the pores predictably have a cylindrical shape open on both ends, which is also shown through TEM imaging (Figure 17).[67]

Ensuing oxidation, as expected, the surface are of the pristine mwcnts increases, whilst the pore volume diminished.[68] This was expected, and confirms the effectivity of the HNO_3 assisted oxidation procedure used. The increase in surface area can be attributed to the cutting and opening of MWCNTs, thereby enabling fluid access to the inner section (Figure 4).[69] The process also forms a larger number of mesopores, exposing new surfaces which were previously inaccessible for reaction due to forming part of the graphene MWCNT wall (Figure 5). Mesopore volume loss is the most prominent change between the Mw and the Ox supports following reflux. Mesopore diameter ranges from 2 to 50 nm which is also the range for the nanotube diameter in MWCNTs.[70] Shorter nanotube segments hold less liquid compared to a continuous tube, hence the dip in pore volume (Figure 5). The relatively small number of macro- and miro-pore volumes remain largely unchanged.

After incipient wetness impregnation, the presence of metal particles adhered on/ in the supports decreased the overall surface area, and pore volume for the majority of the prepared catalysts. Catalysts which underwent selective deposition by pore blocking and washing with Milli-Q®water, i.e. 1I18, 1I7, and 1I7c, had a pore area on par or greater to that shown by Ox. This will be further explained in section 4.5 where TEM images shed more light on these findings. The other catalysts which did not undergo a washing step, have a surface area less than the bare support, and this is reasonable considering that after deposition, metals occupy space on the support, and block N_2 from binding during physisorption measurements. Considering that the mesopore metrics correspond to the inner area of the MWCNT, the decrease in area and volume indicate the presence of metal particles in this region. A relationship appears to be present between these dimensions and the wt% loading, with higher wt% preparations having the lowest total area and volume.

4.3 Support thermal stability

Using Thermogravimetric analysis (TGA) accompanied by gas-chromatography mass-spectrometry, the change in mass with applied temperature was investigated, accompanied by the analysis of products volatilized at each temperature. This allowed for the determination of the thermal stability of the supports (Figure 13), and the ms plot proved useful in establishing a reliable heat-treatment profile (Figure 14). Bare supports had good thermal resistance with thermal decomposition taking place above 600°C. The support with metal present showed steady but gradual drop in mass until a small plateau at the range of 280 to 380 °C, after which it quickly decomposes until a steady weight corresponding to the total metal wt% loading.

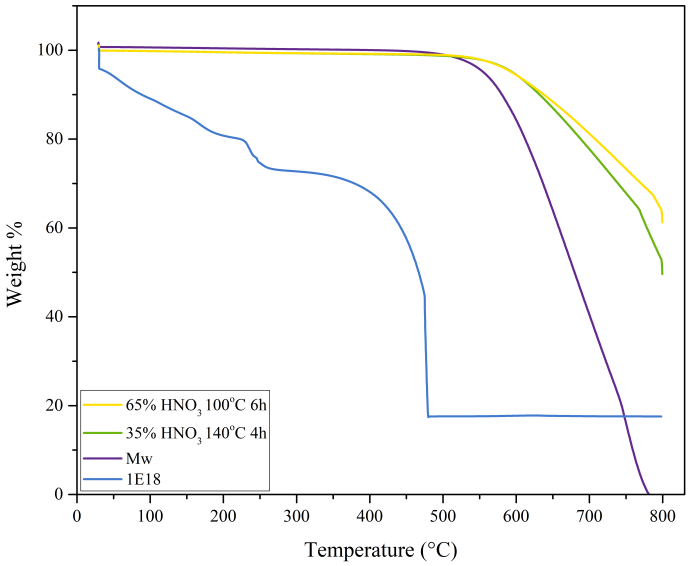

Figure 13: Thermogravimetric analysis plot for metal-free supports analysed in pure Ar, and un-reduced 18 wt% prepared catalysts subjected to TGA in 20 vol% O_2/Ar.

Metal free MWCNTs show a linear decomposition after exceeding 600°C, similar to findings by Mahajan et al. (Figure 13).[57] HNO_3 oxidation appears to not have any detrimental effect on the stability of the material, with thermal decomposition taking place well above the target reaction temperature of approximately 300°C. It is an important note that these promising results, thus far do not fully represent the real experimental conditions. Methanol synthesis conditions involve high pressures which can lead to the premature decomposition of the supports. The lower thermal stability of 1E18 might be due to the Cu/Zn metals. This aligns with findings by Rodriguez et al. which reported that metals adhered onto MWCNTs are able catalyse the thermal decomposition of the support.[30] This would also explain why the oxidized supports have a higher resistance to thermal degradation, since the refluxing step should have removed any trace metal impurities from the production of MWCNTs.

The spectra corresponding for the decomposition products (Equations 7, 8), were overlayed on the 1E18 TGA plot to facilitate the visualization of its thermal decomposition(Figure 14). The 18 AMU spectrum shows two major peaks in the 1 to 100°C range which most likely are the culprit for the loss in mass in 1E18 at that corresponding temperature range (Figure 14a). The origin of the 18 AMU signal is most likely water, which is present as the incipient wetness impregnation solvent, and atmospheric water adsorbed on the acidified support.[71]

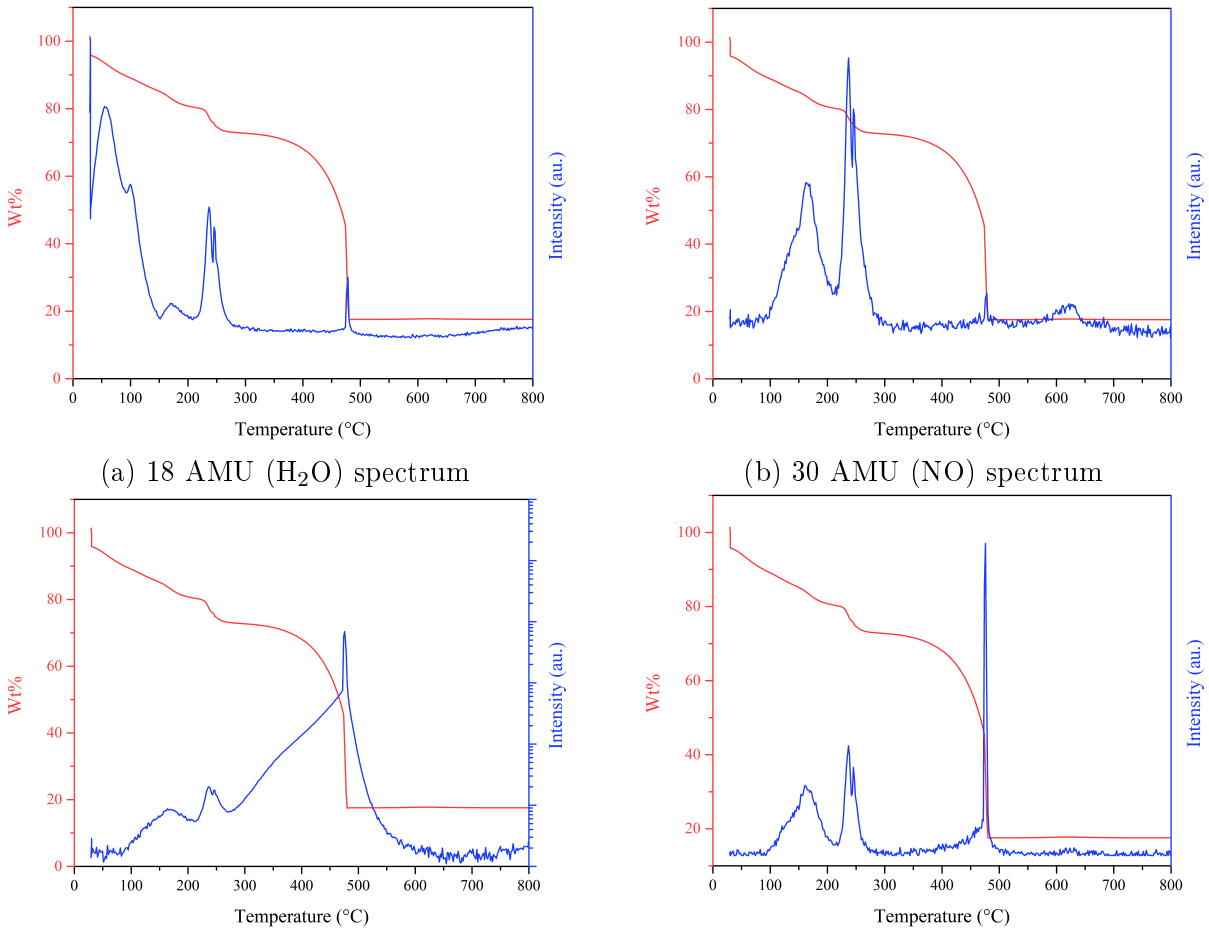

(a) 18 AMU (H_2O) spectrum

(b) 30 AMU (NO) spectrum

(c) 44 AMU (N_2O) spectrum

(d) 46 AMU (NO_2) spectrum

Figure 14: GC-MS spectra of emissions produced during the thermal decomposition of an oxidised MWCNT support deposited by Cu/Zn nitrates (18/7 wt%) under 20 vol% O_2/Ar.

All spectra corresponding to metal nitrate decomposition, show a peak at approximately 250°C (Figures 14b, 14d, 14c). This is similar to findings observed by Małecka et al. when examining the decomposition of metal nitrates deposited onto alumina.[55] They also reported that the thermal decomposition temperatures of Cu and Zn nitrates are analogous, and this is represented in the data especially considering that there is only one sharp drop in wt% at this temperature range. Had the nitrates decomposed at different temperatures, multiple troughs would have been observed. The gas chromatograph for the 44 AMU is of particular interest since this corresponds to CO_2, the major MWCNT decomposition product, and NO_2, a metal nitrate decomposition product (Figure 14c). Through use of a logarithmic scale, observation of both the CO_2 peak at 500°C and the 250°C N_2O peaks is possible. The combination of nitrate absence as well as material stability at the temperature range of 280 to 380°C made it the ideal choice for carrying out heat treatment.

4.4 Metal composition

X-ray diffractograms of pristine MWCNTs, oxidised supports, and prepared catalysts were obtained to analyse the phase of the metals present on the surfaces, as well as to compare between the different wt% loadings (Figure 15). Metal-free supports have identical diffractograms, with peaks corresponding to MWCNTs only (Figure 15a). Apart from the MWCNT preaks, catalyst diffractograms all had peaks corresponding to CuO, and ZnO, with the CuO being more prominent due to its larger concentration during the preparation of the incipient wetness impregnation solution. Catalysts produced with a solution of lower Cu wt% had overall smaller sized CuO peaks (Figure 15b).

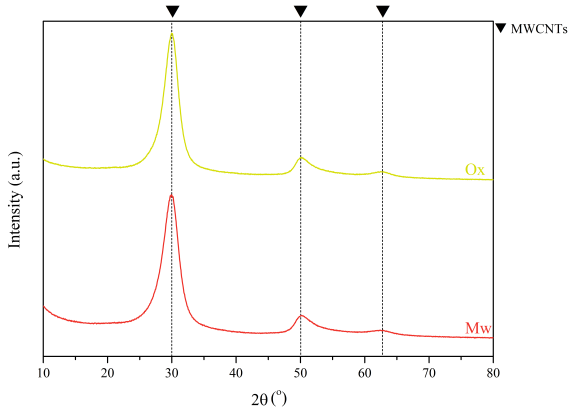

(a) Metal-free supports.

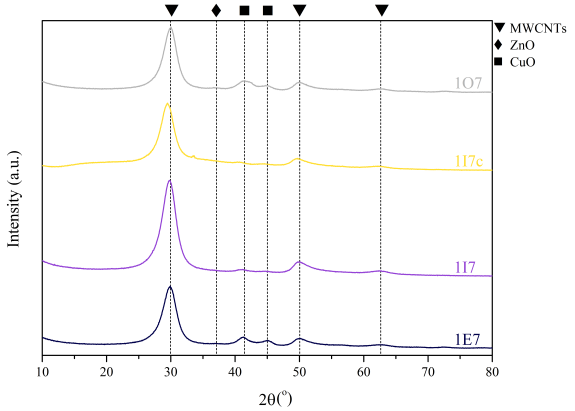

(b) Catalysts prepared with 7.2 wt% Cu.

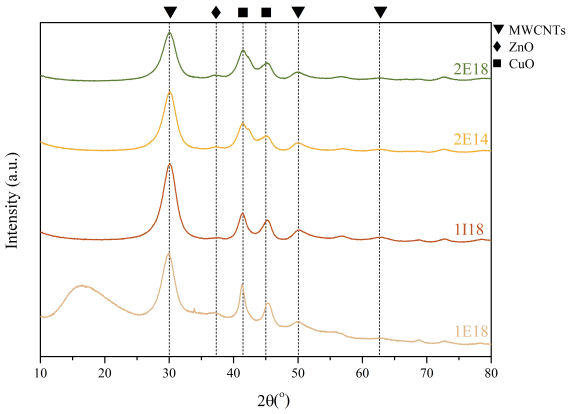

(c) Catalysts prepared with 14.4+ wt% Cu.

Figure 15: X-ray diffractograms taken with CoK$\alpha_{1,2}$ radiation (λ = 1.79026 Å) source.

The absence of any form of metal in the Mw diffractogram show that the supports were free from any trace metal impurities. This information explains why the TGA results for prisine and oxidised supports were virtually identical (Figure 13), since if there were any metal traces, these would have rapidly catalysed the thermal decomposition of Mw.[30] The results also show that activation and acidification of the supports quantified by titration and physisorption did not come at the cost of completely breaking down the MWCNT structure. Accounting for the different radiation sources between the instrument used here and elsewhere, the peaks are in similar ratios to observations by Abdullah et al.[72]

The high temperature, oxidising conditions the supports were subjected to during preparation had the potential to damage or destroy the MWCNT structures.[55] XRD analysis of the catalysts proved otherwise and the peaks corresponding to MWCNTs were present here just as they were in the metal-free supports (Figures 15b & 15c). Cu and Zn were found to be in the oxidized form, hence the oxidation step carried out was effective (Section 3.3.5). The plots are similar to those of Cu/Zn loaded CNTs produced by Shahsavar et al.[52] As expected, the metal oxide peaks intensity corresponds to the wt% of the loading solution. Facet identification was carried out the oxidised catalysts, with all of them showing the same results. To illustrate the observations, below the is the facet-labelled 2E18 diffractogram (Figure 16).

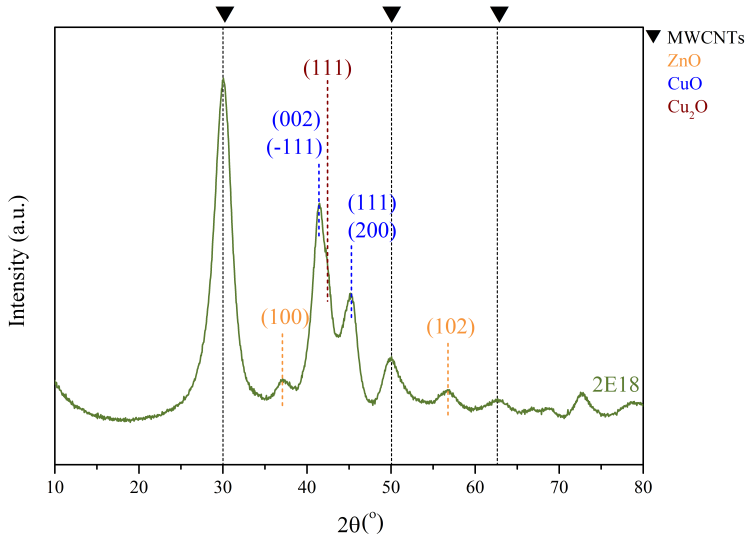

Figure 16: X-Ray diffractogram of 2E18 with the facets for the metal oxides identified.

Through comparison of the measured diffractogram with the material database a number of different facets were identified. Interestingly, the 111 facet for Cu_2O was found, but this overlaps with the larger 002 and -111 peaks. Although the presence of these facets is interesting, this is not really relevant for catalysis, since the in-situ reduction steps converts all the oxides into metals into their elemental form. To identify which catalytically active facets are present, the catalysts would need to be analysed in their reduced state, either in an operando setup, otherwise by assembling a *dome* XRD holder under inert conditions immediately after reducing under H_2.

4.5 TEM

TEM enabled for the observation and comparison of the changes brought about by the oxidation process and the deposition of the metal nanoparticles to form catalysts. Pristine MWCNTs show long tube structures which feature multi-laminate walls enclosing a continuous inner cavity (Figure 17a). Treating the MWCNTs with HNO_3 and refluxing resulted in shorter tubes, whilst largely retaining the multi-laminate walls, and continuous internal cavity of the structures (Figure 17b). The outcome of the oxidation process performed is similar to observations by Solhy et al.[53] The findings of this project are very similar to the aforementioned project, with prolonged reflux utilising a mild acid concentration resulting in the increase of surface acidity (Figure 11). BET surface area

enhancement as a consequence of the slight damage caused to the overall MWCNT structure is another similarity (Table 5, & Figure 18a). The nature of the surface groups present on the Ox cannot be definitively assigned since no surface analysis techniques such as Raman were performed.[73]

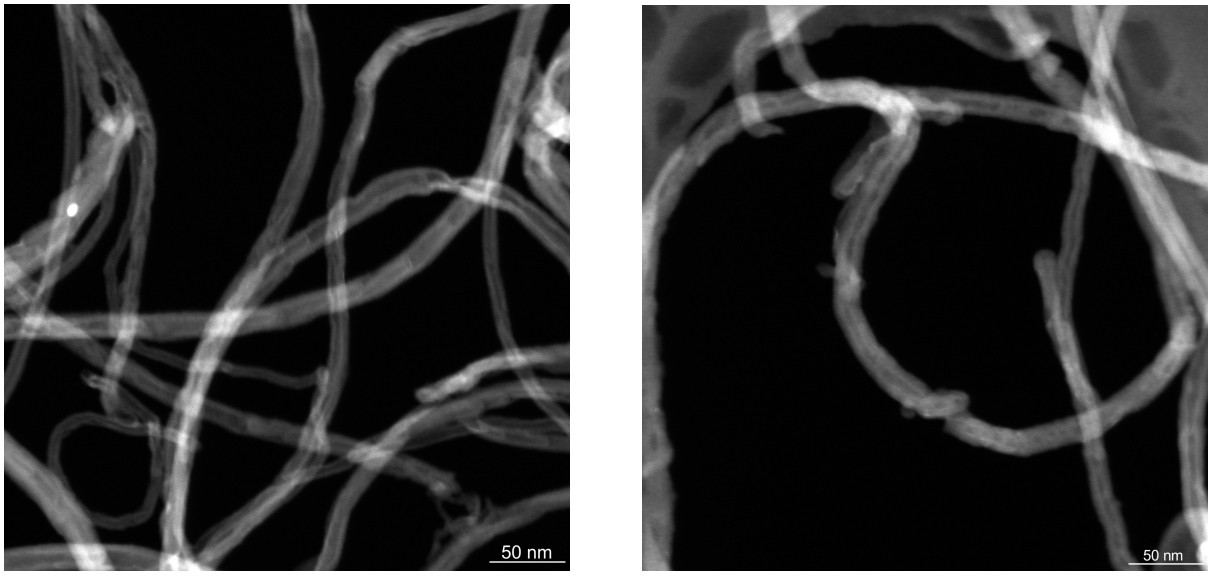

(a) Pristine MWCNTs (Mw) (b) HNO_3 oxidised MWCNTs (Ox)

Figure 17: Transmission electron micrographs of metal-free supports observed at 270k magnification.

1E7 has a large number of metal nanoparticles present inside the nanotubes which is quite interesting considering that the metal impregnation procedure employed no selective deposition techniques (Figure 18a). The second image of note is the 1O7, which underwent selective deposition favouring the external surface (Figure 18d). From the TEM images, it can be seen that the metal particles are found inside the MWCNT, hence the method used to selectively target the convex surface was not only unsuccessful, it produced the exact opposite to what was desired! 1I7 and 1I7c were both prepared using an adaptation of method iii presented in section 1.5.1 (Figures 18b & 18c respectively).[50] 1I7c had no n-hexane to block the inner surface so it can be assumed that the water was able to dissolve all the deposited Cu and Zn nitrates. 1I7, which used n-hexane to block its pores, appears to still have some metal particles present, albeit nowhere close to 1E7, and 1O7. 1I7 and 1I7c produced an underwhelming XRD plots especially when viewed with their cohort (Figure 15b). The only way to view any trace of Cu/Zn is to view them on their own (Figures 27f, & 27g respectively). Unsurprisingly, the catalysts which showed the most prominent metal particles are also the ones which have the highest peaks in their corresponding XRD plots (Figure 15b).

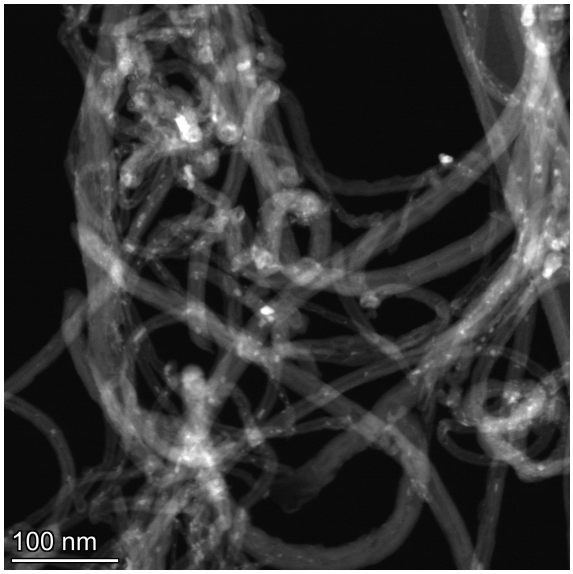

(a) IE7

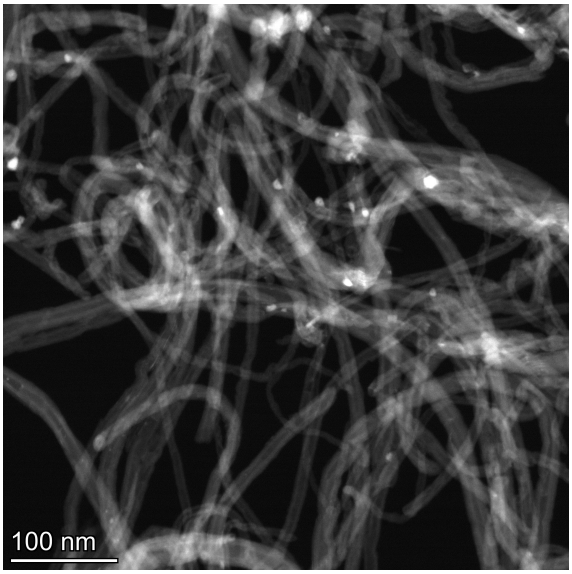

(b) 1I7

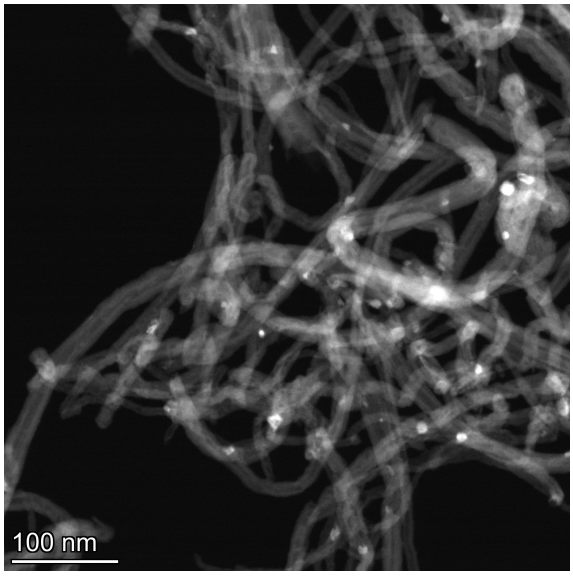

(c) 1I7c

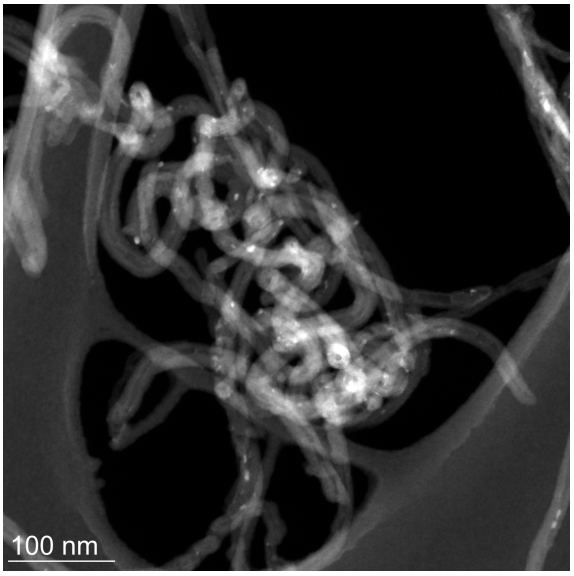

(d) 1O7

Figure 18: Transmission electron micrographs of catalysts prepared using a 7.2 wt% Cu loading, heat-treated and oxidized, observed at 135k magnification.

Across all the prepared catalysts, TEM observations showed that metals were present on the MWCNTs (Figures 18 & 19), the nature of which was investigated through XRD (Figure 15). Naturally, catalysts prepared with solutions to achieve a lower Cu wt% loading, also had less metal particles present throughout. 1E7, the catalyst prepared by incipient wetness impregnation only, had a good distribution of metal particles, with the majority having a small size and appear to be located within the internal channel of the MWCNT (Figure 18a). Due to the overall smaller particle size, this catalyst benefited from a very small reduction in surface, and an equal pore volume compared to the initial support (Table 5). 1I7 and 1I7c both underwent the same selective deposition procedure, with the latter acting as a control for the former thus undergoing washing without a protecting solvent. The micrographs for both show similar particle quantities, and their size is as big as the nanotubes (Figures 18b, & 18d). From physisorption measurements,

these catalysts have very high mesopore surface area and volume, suggesting that the deposited metal is mostly adhered to the outer convex surface of the MWCNT and not present inside. As such this means that the attempts made to restrict metal exclusively to the inner surface of MWCNTs was unsuccessful. 1O7 underwent an initial pore-blocking, and then incipient wetness impregnation to achieve a metal deposition only on the outer surface. The metal particles on the support all have a small size, and they are present over all of the support (Figure 18d). From physisorption, we can draw the assumption that these particles are present within the MWCNTs dur to diminished micropore area and volume (Table 5).

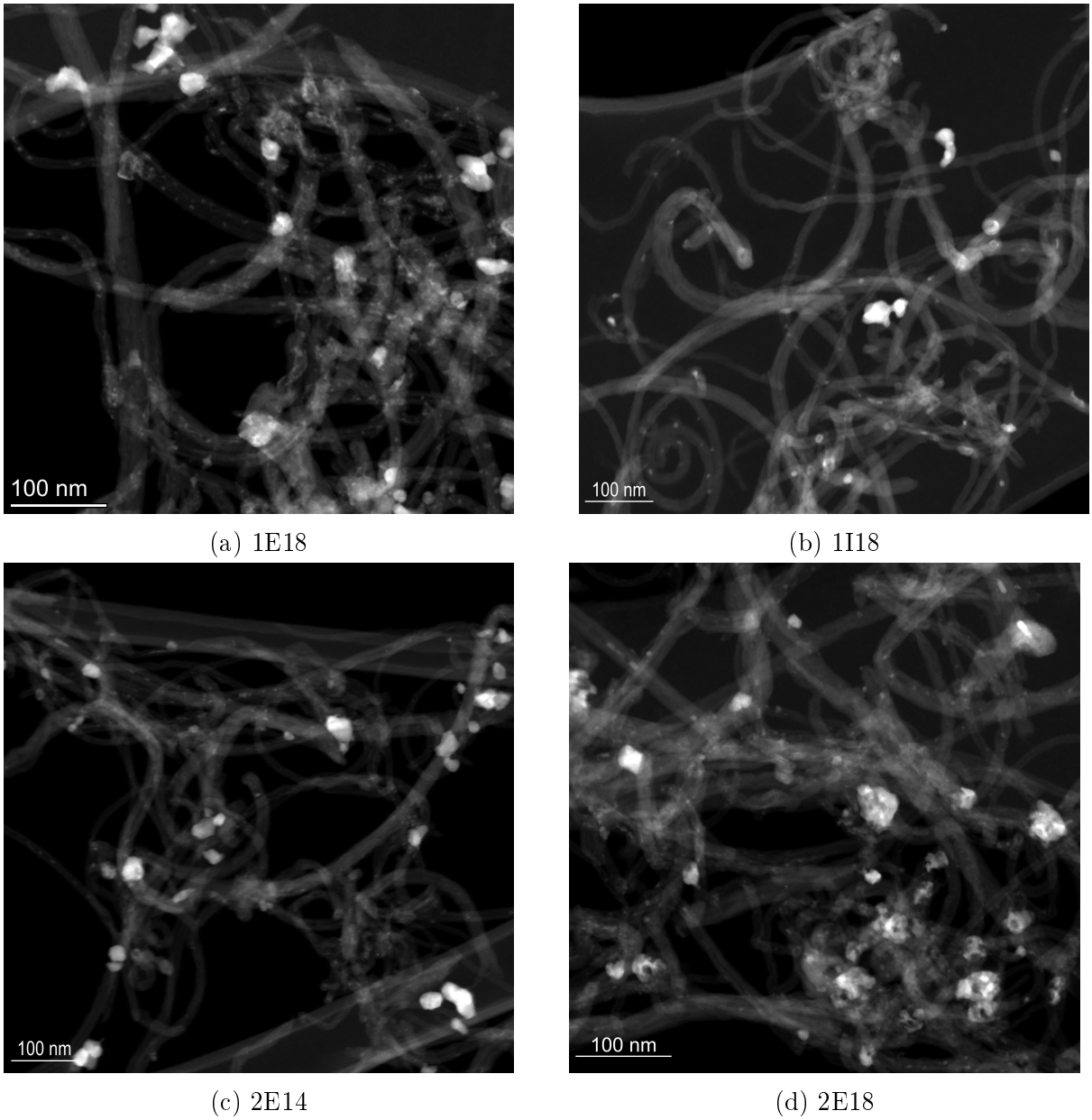

(a) 1E18

(b) 1I18

(c) 2E14

(d) 2E18

Figure 19: Transmission electron micrographs of catalysts prepared using a Cu loading of 14.4+ wt%, heat-treated and oxidized, observed at 135k magnification.

Catalysts prepared using concentrated (14.4 wt%+) solutions, all showed some degree of clustering (Figure 19). 1E18, similar to its lower concentration counterpart in the form of 1E7, also showed a good particle distribution, with both large and small particles being present here (Figure 19a). The presence of large clusters is expected for the 18 wt% Cu preparation, since these systems are prone to particle growth when heated.[74] The area and volume dimensions for this catalyst are greatly reduced in comparison to the starting support, leading to the assumption that metal particles are present over both convex and concave MWCNT surfaces. 1I18 also shared similarities with its lower wt% counterpart 1I7, with the former having the majority of the metal found as large clusters (Figure 19b). The large clusters are adhered to the outer surface, based off the fact that they are too large to fit within the inner MWCNT surface, as well as a high mesopore area for the catalyst (Table 5).

The last two catalysts, 2E14 and 2E18, underwent a deposition to achieve a high wt% loading, but using two applications of lower concentration solutions with a drying step in between (Figures 19c, & 19d). Both catalysts show large clusters adhered to the external surfaces, as well as a number of smaller sized metal particles present within the inner area of the MWCNT, with 2E18 having a larger quantity of internally bound particles compared to 2E14 (Table 5). These catalysts were prepared in an attempt to emulate the metal particle distribution and size seen in 1E7, but without the large clusters seen in 1E18. The idea was that any deposition shortfalls brought about by the viscosity of the solution used for incipient wetness impregnation could be overcome by using two less viscous solutions of lower concentration.[75] This methodology adopted appears to be unsuccessful, since these supports lack both the small particle size of 1E7, as well as the more thorough particle distribution of 1E18.

Looking at the supports which underwent selective deposition as a whole, i.e. 1I7, 1I7c, and 1I18 (Figures 18b, 18c, & 19b), the results indicate that the method was flawed and it resulted in particles being large (Figure 20), and present mostly on the external surface of the MWCNTs. The publication used to base the methodology off of is just one of many, and perhaps a different approach might be able to achieve a better particle distribution whilst retaining an metal-free external surface.[38,44–50]

4.6 Elemental analysis

To accurately quantify the actual wt% of the metal loading following preparation, and verify the validity of the methods, Energy-dispersive X-ray (EDX) analysis was used. The measured results are compared to the intended wt% loading in the below table (6).

Table 6: Experimentally measured wt% loadings for the catalytically tested supports.

Catalyst	**Theoretical (wt%)**		**Actual (wt%)**		**Change (%)**	
	Cu	**Zn**	**Cu**	**Zn**	**Cu**	**Zn**
1E18	18	7	13.9	8.07	-22.8	15.3
1E7	7.2	2.8	4.81	0.89	-33.2	-68.2
1I7	7.2	2.8	5.68	0.62	-21.1	-77.9
1I7c	7.2	2.8	4.33	0.21	-39.9	-92.5
1O7	7.2	2.8	5.07	1.54	-29.6	-45.0

In comparison to the deposited quantity of copper, the finished catalysts all ended up with a diminished wt% with a discrepancy of a 20% or more. With the exception of 1E18, the zinc showed the same trend, albeit at a greater decrease in wt%. The trends observed here align well with XRD and TEM analysis, both of which exhibited a lower presence of metal than expected, especially for supports prepared with a 7.2 wt% solution (Figures 15, 18, & 19a). The reason for the increase in wt% observed in the 1E18 may have come to be as a result of the support decomposing during heat treatment. As was seen in TGA, well deposited metal particles remain largely unaffected since they are not pyrolyzed the same way the carbon support is (Figure 13).[57]

These results also show something which warrants further explanation. All the 7 wt% catalysts prepared and presented in the above table were prepared using the same solution, with the difference being the procedure applied to achieve a surface biased deposition. 1E7 and 1E18, showed deviation of more than 20% for the Cu wt%, yet they underwent no washing steps. This means that the losses cannot be explained away due to being removed by a water washing step, but these losses are due to other factors. Projects which make use of this deposition technique do not give any information regarding measuring the actual deposited metal content.[76–80] This lack of information could be either due to oversight on their part, or the more likely situation of working around an already accounted for loss factor. Since the deposition procedure involves several experimental steps, it is rather difficult to pinpoint the exact culprit for the loss, with many transfer steps being a possibility, as is initial losses due to liquid remaining in the syringe, or slight deviations in the support mass when estimating the volume of required liquid. The small mass of support and volume of liquid used here also hinder the final result since even small errors manifest into significant losses.

The porosity of the MWCNTs used is not perfectly homogenous, so the fluid uptake may not be complete. Surface adhered metal is easier to dislodge and lose upon contact with the glassware prior to heat-treatment. Some improvements can be made by doing multiple incipient wetness-impregnation steps following an identical procedure, then through EDX or TGA, a *loss factor* can be found, which can then be integrated into the wt% loading calculation to achieve a desired wt% in spite of losses.

4.7 Particle size analysis

Using imageJ, the metal particles were measured from the TEM images. The tabulated results were then plotted in the box and whisker diagram presented below (Figure 20). The majority of the catalysts had a large range of particle sizes, with the smallest distribution being that of 1E7, and the largest of 1E18. 1E7 also had the smallest mean particle size, with the largest mean particle size found in the 2E14 catalyst.

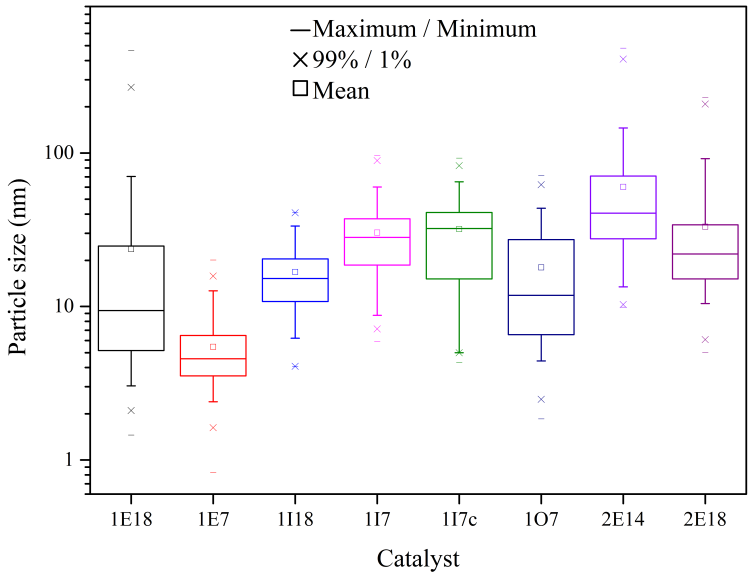

Figure 20: Plot showing particle sizes as a result of different wt% loadings and deposition techniques. The line bisecting each box is the median, the box represents 25 to 75% of the data, and the whiskers represent 5 to 95% of the dataset.

Catalysts prepared by the selective deposition method, all had mean particle sizes which were in a close range to one another, but all were larger than 1E7. Their distribution was not so big as others, with the majority of the data being clustered around the median. 1O7, ie. externally favoured loading catalysts resulted in quite a large data distribution as well as a large particle size. It is expected that if particles are present on the external MWCNT surface, they become larger, however the data distribution also dips below 10 nm meaning the particles were inhomogeneous. The large average particle size of 2E14 and 2E18 indicate that the majority of the particles are present on the external surface. It is interesting to note that although 2E14 underwent the same treatment as 1E7, just with an additional loading step, they share little similarities, with the majority of the data ranges having barely any overlap. This meant that during preparation of 2E14, at the second deposition the new solution might have had an interaction with the already 'in-place' metal nitrates, which could have had an influence over the movement and final result of the metal particles.

4.8 Catalyst behaviour under reducing conditions

To analyse how the catalyst behaved under reducing (experimental) conditions, it was subject to H-TPR. The results for this would also aid in setting up reaction conditions down the line, experimentally obtained data is presented in figure 21.

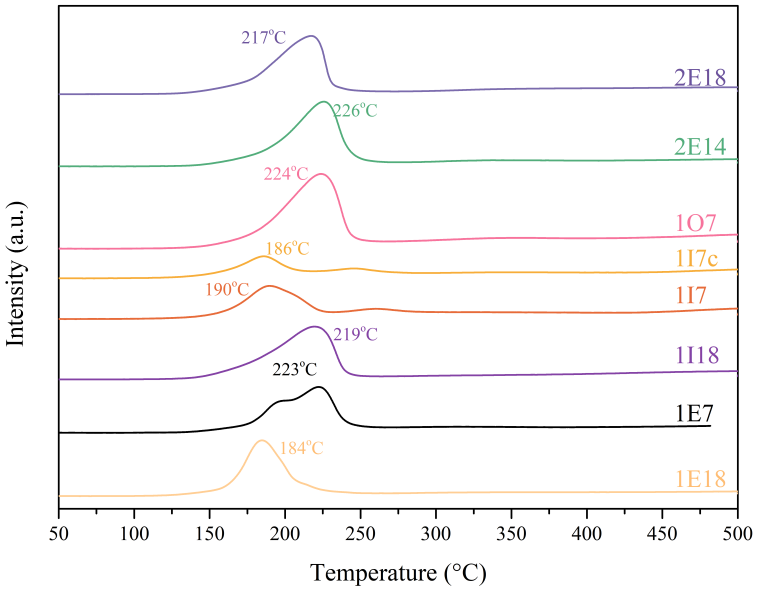

Figure 21: Temperature-programmed reduction for the oxidized catalysts under a 5% H_2/Ar atmosphere.

All the TPR peaks fall within the range of 184 to 226°C (Figure 21). The reduction temperatures are similar to those obtained by Grossman et al. who carried out similar testing using Cu/Zn on CNTs.[44] The measured reduction temperatures meant that protocols utilizing commercial CZA for methanol formation could be emulated more closely since these used an *in situ* reduction step prior to commencing catalysis at 250°C.[81–83] There seems no correlation between the deposited wt% and the reduction temperature, which is unlike what was observed by Kundakovic et al.[84] Panagiotopoulou had previously reported that metal particle size is correlated to the reduction temperature, with smaller particles being reduced at lower temperatures in contrast to their larger counterparts.[85] This was also not observed in these results, with 1E7, which had the smallest average particle size (Figure 20), having one of the highest reduction temperatures at 223 °C.

4.9 Catalytic activity

Analysing the CO and CO_2 content in the effluent gas stream via on-line GC and comparing it to the input volume gives the time resolved percentage conversion for the catalysts tested (Figure 22, Table 7). When the plot was constructed, only *successful* catalysts were used (conversion $\geq$ 2%). The general trend is that as the CO_2 concentration is increased, the conversion also increases. This is very much in line with findings reported by research carried out by Zhang et al. who reported that the individual rates for methanol formation using CO or CO_2 as feedstocks is much lower than using a mixed feed.[86]

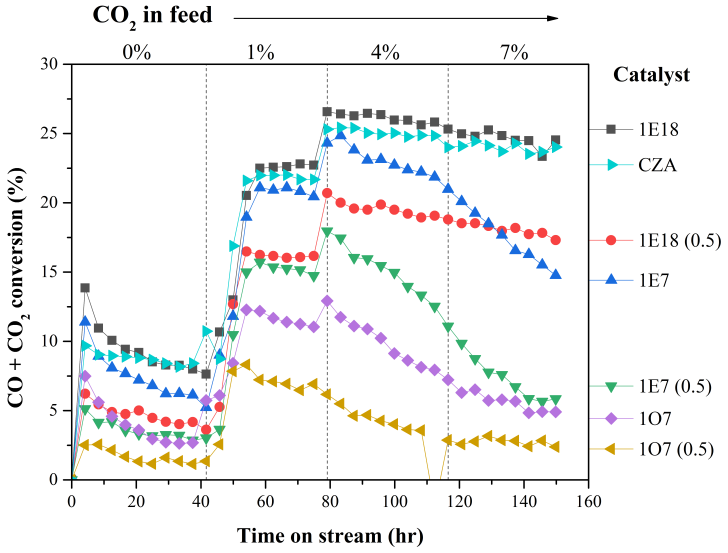

Figure 22: Time resolved of CO+CO_2 conversion from on-line GC-MS. 15mg of CZA was used, 30 mg was used for catalysts marked with 0.5, 60 mg was used for the remainder.

The CO_2 free feedstock exhibited conversion in the range of 10% for the best performing supports. A CO-only feed has low conversion due to weak binding of the carbon to the ZnO, where the ZnO actually blocks the Cu binding sites.[29] In this situation, a Zn free catalyst would have most likely fared better. Once CO_2 is introduced it is a totally different situation, with all the conversions immediately doubling, due to the the shift from CO to CO_2 as the main carbon source and it being able to destroy the formate intermediate (Equation 4).

Increasing CO_2 feed concentration to 4%, two different patterns emerged. The catalysts prepared to have a 7 wt%, had their conversion decline which their performance just before the end of the test having decreased by a minimum of 25% relative to their peak conversion. The trends shown at a CO_2 concentration of 1% are too small to determine if this is due to the feedstock composition or due to deactivation. Since the gas feed is sulfur and chlorine free, the main ways these catalysts can deactivate is through particle growth.[74] It is well known that smaller particles are more susceptible to this type of deactivation, and from TEM and particle size measurements it was seen that these catalysts had some of the smallest average particle size (Figures 18a, 18d, & 20).[87] Particle growth requires several conditions to occur, with the most important parameter being an elevated temperature, in order to overcome high activation energy. Sustained high temperature and pressure conditions which are required for methanol synthesis are also conducive to deactivation. For 1O7 specifically, due to its larger particle size distribution compared to 1E7, it might be even more prone to Ostwald ripening, a mechanism by which smaller particles are attracted towards larger clusters, and then coalesce once close.[88]

The 1E18 support, both the 60 and the 30 mg, showed good sustained performance with an increase in conversion over the 1% CO_2 concentration. Predictably, the CZA followed suit, and was on par with the performance of 60 mg 1E18. It is important to mention here that this plot does not account for the Cu wt% loading, nor does it account for the mass

of catalyst performance, so in reality, on a gram for gram comparison, CZA is 4 times as capable as the 1E18. With that in mind, there seems to be some limitations which are hindering the catalytic performance of the 1E18. The prepared reactor tube with 30 mg IE18, which had effectively double the GHSV showed a conversion rate of approximately 20% compared to that of 25% exhibited by the 60 mg 1E18. This had a conversion rate higher than the 50% drop expected based off the mass used within reactor. There are two possible explanations for this observation:

i The conditions chosen are *one size fits all*. They favour methanol formation for all catalysts by having a slightly longer contact time between the feedstock and the catalyst. The problem with this approach is that the GHSV is not rapid enough to clear out the methanol to make use of all the copper present on the catalyst. This leads the catalyst to hit a plateau, as is seen in the plot, and to proceed further it requires a more rapid gas flow.

ii Conversions above 25% are thermodynamically unfeasible. Adding copper results in diminishing returns, whilst altering reaction conditions reduces methanol selectivity.

To help answer this question, we can take a look at the copper time yield (CTY) and the activity plots for the catalysts presented below (Figure 23). Both of these plots use the same experimentally collected measurement, which is the consumption of CO and CO_2 per unit time, the difference lies in the lens by which we compare the catalysts. CTY focuses on the copper component of the catalyst, and as such it uses the wt% loading in conjunction with the mass of catalyst used to calculate the consumption of CO and CO_2 per gram of copper per second. Activity measurements only require the mass of the catalyst used.

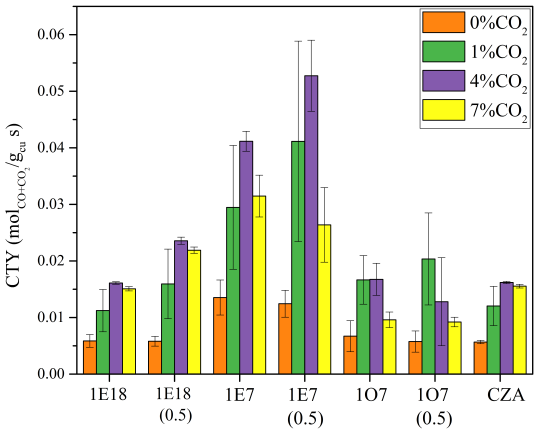

(a) Plot of average copper time yield for each catalyst composition at the different CO_2 concentrations. Error bars represent standard deviation. 0.5 represents the use of 30 mg of catalyst, 15 mg of CZA was used, for the rest 60 mg was used.

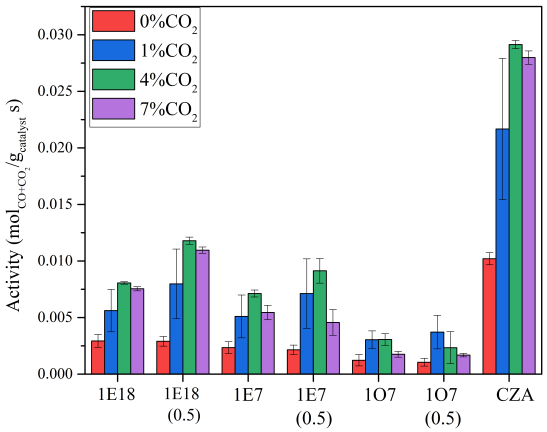

(b) Plot of average activity for each catalyst composition at the different CO_2 concentrations. Error bars represent standard deviation. 0.5 represents the use of 30 mg of catalyst, 15 mg of CZA was used, for the rest 60 mg was used.

Figure 23: Bar plots of Copper time yield, and Activity for the catalysts during methanol formation testing

At a cursory glance, the plots appear to be the exact opposite of one another, with the largest peaks in the CTY plot arising from the 1E7 catalyst (Figure 23a), and the largest peaks by far in the activity plot belonging to the CZA (Figure 23b). Density is what gives these results context and meaning. In the case of CTY, a less dense catalyst, hence one with a much lower wt% loading performs much better. To end up with an equal mass of copper you would need to use approximately 2.6 g of 1E7 for every 1 g of 1E18. 1E7 is a much more well-dispersed catalyst compared to 1E18, hence it has better CTY performance in comparison (Figures 18a vs 19a). Activity, on the other hand, uses the mass of the catalyst as a metric, so this favours a higher wt%. 7 and 18 Cu wt% depositions on MWCNTs do not produce catalysts which are vastly different to one another in terms of mass, whilst the 40+ wt% Cu of CZA makes for a denser catalyst which is more active per gram in comparison to the MWCNT supported ones produced in this project.

1O7 has poor performance in both CTY and activity plots, so this can be ruled out as an inadequate catalyst, allowing us to focus on 1E18 and 1E7. All the plots indicate that a 4% CO_2 concentration in the gas feed produced the best results, and had some of the most consistent measurements with the standard deviation being among the smallest in relation to the size of the average. This is very much in line with findings made within the group were it was reported that for 2-dimensional graphitic supports, the best performance was found at a CO_2 concentration of 3%.[89] The increase in CO_2 results in the formation of water as a byproduct (Equation 5). This water is them consumed in the water gas shift as well as in the formation of methanol on the ZnO leaving an OH group adsorbed on the surface (Equation 6). Lastly this adsorbed OH group is consumed to form an adsorbed O group (Equation 4). The final result of this over sustained reaction cycles is that slowly, if there is a high concentration of CO_2 present, surface bound O groups start accumulating. These oxidize the catalyst and slowly deactivate it. It can be seen very clearly that after increasing the concentration from 4 to 7%, the downward trends which started at 4% CO_2 concentration, increase in pace (Figure 22).

Circling back to the hypotheses made above, it appears that theory ii is most likely the correct explanation. The catalytic activity of the 60 mg catalyst reactors vs the 30 mg counterparts is only marginally better (Figure 23b). This does not mean that theory i has no merit. On the contrary, comparing the CTY of 30 mg 1E18 and 60 mg 1E7 is a quite evenly matched comparison in terms of Cu content. A more dispersed support, with smaller sized nanoparticles located in the inner cavity, appears to make much better use of its deposited copper in comparison to a catalyst with large clusters of metal adhered to its convex surface (Figures 18a, & 19a). The disadvantage to 1E7 is that due to its low particle size and close particle proximity, it is very susceptible to deactivation. 25% being the conversion ceiling is also backed up by similar projects, where the majority found that the maximum conversion hovered around this figure.[40,42] Dong et al. managed to push conversion higher than 25% by the use of Al promoters, and catalyst preparation through co-precipitation.[35,41] The last measurement to look at is the selectivity of these catalysts, and this is displayed in the below plots (Figure 24).

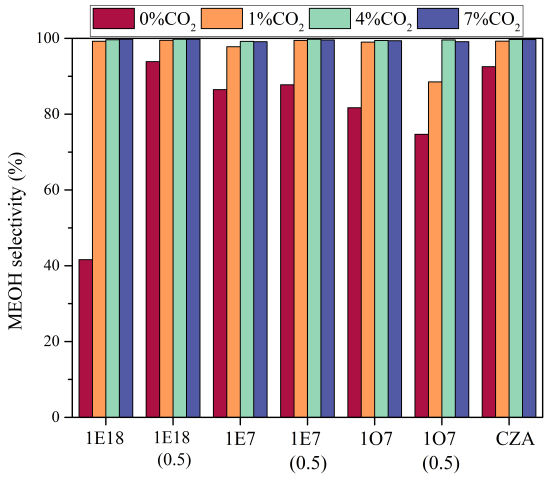

(a) Selectivity of methanol (MEOH) for the prepared catalysts.

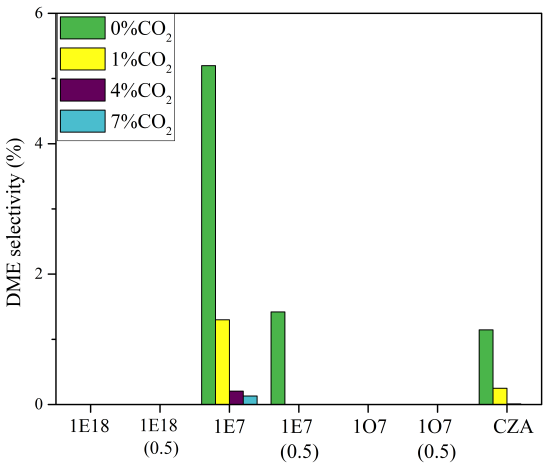

(b) Selectivity for dimethyl ether (DME) across the prepared catalysts

Figure 24: Selectivities for the two most prominent products

As expected, under the conditions used in the Flowrence II test, the Cu/Zn catalysts made almost exclusively methanol (Figure 24a). In the absence of CO_2 the catalysts' methanol selectivity was low. The catalysts do not function properly without an adequate concentration of CO_2, and all the previous attest to this. [29] Once the feedstock incorporated 1% of CO_2, the methanol selectivity immediately increased to above 80%. Subsequent increases enabled the selectivity to reach 100%, where it remained for the duration of the catalytic test. This test showed that the proximity of Cu and Zn is good enough for the reaction to proceed and they can work in tandem to carry out the reaction.[28] Dimethyl ehter formation requires strong acidic groups to dehydrate the methanol.[5] When the supports were being processed, the oxidation via nitric acid did add acidic groups (Figure 8).[63] These acidic groups were then lost during the heat-treatment steps and the catalyst ended up being slightly basic (Figure 11). The basic nature of the catalysts explains why the dimethyl ether selectivity is abysmal, with the best result being a selectivity of 5% for 1E7 with the CO_2-free feedstock. Commercially, to produce dimethy ether from CO/CO_2, to mix in HZSM-5 with the Cu/Zn catalyst, which serves to dehydrate the freshly formed methanol into DME.[82] Compared to similar catalysts, the absence of any other metal or acid sites allowed it to be highly selective for methanol production. Upon the addition of promoters such as Zn or Zr, C_{2+} products are formed which is beyond the scope of this project.[42,43]

5 Conclusion

From the several catalysts prepared, it was found that preparations using a straigforward incipient wetness impregnation using Cu wt% of either 7.2 or 18 had overall the best results. There appeared to be a significant discrepancy between the desired wt% loading and the actual wt% which was confirmed through EDX. Attempts made to prepare catalysts with metal particles present on only one of the two surfaces proved to be unsuccessful, with these catalysts also not being active enough to be feasible. The produced catalysts had the best performance at a CO_2 concentration of 4% with good stability especially for the Cu 18 wt% preparation. All the catalysts formed methanol as the sole product, with no dimethyl ether due to the removal of acid groups by the high temperature conditions. The 7.2 wt% catalyst appeared to have a larger portion of its metal

6 Outlook

Throughout the project several new research questions arose which themselves appear to be gaps in the knowledge spanning further than MWCNTs as supports. One of these is the viscosity as a parameter which arose due to creating high wt% solutions. The solvent used for blocking the inner pores and protection of the deposited metal was not a good fit. An improvement to this may be to use a protecting solvent that is injected while warm, which then turns into a gel-like consistency once cooled, preventing water entry into the pores. Another possible approach is to immediately freeze the supports following incipient wetness impregnation to lock the water inside the pores and carry out low temperature washing at or below 5°C, minimizing heat transfer between the protecting and washing solvent.

Since the catalysts placed at 30 mg still showed good results, another catalytic test should be attempted using a GHSV double the one used in this project. This would enable us to compare the catalysts at a relative GHSV of 1, 2, 4. This increased flow should also prove for sure if there are any limitations hindering the catalysts from reaching their maximum CO and CO_2 conversion. A flaw in the project as it stands is that the spent catalysts following the completion of a reaction cycle were not examined in any way nor was their catalytic ability retested. TEM would provide invaluable insight into the deactivation and the underlying causes for this can be identified and addressed in subsequent catalyst preparations.

Looking at the big picture and the place of this research one can note that studies effectively comparing and contrasting the selective deposition approaches exist, which results in publications making use of one technique over an other a guessing game of sorts. Although the results of this master's project were more skill related, rather than strictly results focused, they do indicate that the research questions posed still have a lot of depth of exploration, and this can also be applied to other carbon products and not exclusively methanol.

7 Acknowledgements

First and foremost I would like to thank my parents, without whose support and sacrifices I would not be at the place where I am today. Secondly, I would like to thank my girlfriend Christine, who was there to endlessly hear my chemistry related comments and complaints.

On a professional level, I would like to thank my supervisors Yuang and Dr. Komal Patil, who took the time to explain to me complex concepts and encouraged me to explore my own path. For making the whole project come together the way it did, I would like to thank Prof. Dr. Petra De Jongh. I would also like to thank all the MCC technical staff who carried out measurements on my samples, kept the equipment running, and their presence and willingness to lend a hand if ever anything went wrong. Lastly, I would like to thank the MCC group as a whole, whose working environment is very positive and made me feel welcome as a foreign student.

I would like to acknowledge and thank the Endeavour II Scholarship Scheme which provided the necessary funds for me to pursue my education at Utrecht University.

References

(1) Beychok, M. R. Coal gasification and the Phenosolvan process. *Am. Chem. Soc., Div. Fuel Chem., Prepr.;(United States)* **1974**, *19*.

(2) Wang, Z.; Yang, J.; Li, Z.; Xiang, Y. Syngas composition study. *Frontiers of Energy and Power Engineering in China* **2009**, *3*, 369–372.

(3) Da Silva, M. J. Synthesis of methanol from methane: Challenges and advances on the multi-step (syngas) and one-step routes (DMTM). *Fuel Processing Technology* **2016**, *145*, 42–61.

(4) Cai, G.; Liu, Z.; Shi, R.; Changqing, H.; Yang, L.; Sun, C.; Chang, Y. Light alkenes from syngas via dimethyl ether. *Applied Catalysis A: General* **1995**, *125*, 29–38.

(5) Saravanan, K; Ham, H.; Tsubaki, N.; Bae, J. W. Recent progress for direct synthesis of dimethyl ether from syngas on the heterogeneous bifunctional hybrid catalysts. *Applied Catalysis B: Environmental* **2017**, *217*, 494–522.

(6) Takeishi, K. Dimethyl ether and catalyst development for production from syngas. *Biofuels* **2010**, *1*, 217–226.

(7) Sheldon, D. Methanol production – a technical history. *Johnson Matthey Technology Review* **2017**, *61*, 172–182.

(8) Sabatier, P.; Senderens, J.-B. *Annales de chimie et de physique* **1905**, *4*, 318.

(9) Alwin, M.; Mathias, P. Synthetic manufacture of methanol, US Patent 1,569,775, 1926.

(10) Teoh, W. Y. Evolution of catalysts design and synthesis: From bulk metal catalysts to fine wires and gauzes, and that to nanoparticle deposits, metal clusters, and single atoms. *Heterogeneous Catalysts* **2021**, 1–19.

(11) Murkin, C.; Brightling, J. Eighty Years of steam reforming. *Johnson Matthey Technology Review* **2016**, *60*, 263–269.

(12) Brown, S. P.; Yttcel, M. K. What drives natural gas prices? *The Energy Journal* **2008**, *29*, 45–60.

(13) Phineas, D.; Forster, S. F. Production of oxygenated hydrocarbons, US Patent 3,326,956, 1967.

(14) Gallagher, J. T.; Kidd, J. M. Methanol Synthesis. GB Patent App. 41002/65 A, 1969.

(15) Appl, M In *World Methanol Conference, Frankfurt, Germany, 15th December*, 1998.

(16) Dasireddy, V. D.; Likozar, B. The role of copper oxidation state in Cu/ZnO/Al2O3 catalysts in CO2 hydrogenation and methanol productivity. *Renewable Energy* **2019**, *140*, 452–460.

(17) Chinchen, G. C.; Denny, P.; Jennings, J.; Spencer, M.; Waugh, K. Synthesis of methanol: part 1. Catalysts and kinetics. *Applied catalysis* **1988**, *36*, 1–65.

(18) Leonzio, G. State of art and perspectives about the production of methanol, dimethyl ether and syngas by carbon dioxide hydrogenation. *Journal of CO2 Utilization* **2018**, *27*, 326–354.

(19) Molina, M. J.; Rowland, F. S. Stratospheric sink for chlorofluoromethanes: chlorine atom-catalysed destruction of ozone. *Nature* **1974**, *249*, 810–812.

(20) Ott, J.; Gronemann, V.; Pontzen, F.; Fiedler, E.; Grossmann, G.; Kersebohm, D. B.; Weiss, G.; Witte, C. Methanol. *Ullmann's encyclopedia of industrial chemistry* **2000**.

(21) Elfasakhany, A. Investigations on the effects of ethanol–methanol–gasoline blends in a spark-ignition engine: Performance and emissions analysis. *Engineering Science and Technology, an International Journal* **2015**, *18*, 713–719.

(22) Kianfar, E.; Hajimirzaee, S.; Mehr, A. S., et al. Zeolite-based catalysts for methanol to gasoline process: a review. *Microchemical Journal* **2020**, *156*, 104822.

(23) Yu, K. M. K.; Curcic, I.; Gabriel, J.; Tsang, S. C. E. Recent advances in CO2 capture and utilization. *ChemSusChem: Chemistry & Sustainability Energy & Materials* **2008**, *1*, 893–899.

(24) Liu, X.-M.; Lu, G.; Yan, Z.-F.; Beltramini, J. Recent advances in catalysts for methanol synthesis via hydrogenation of CO and CO2. *Industrial & engineering chemistry research* **2003**, *42*, 6518–6530.

(25) Ng, K. L.; Chadwick, D; Toseland, B. Kinetics and modelling of dimethyl ether synthesis from synthesis gas. *Chemical Engineering Science* **1999**, *54*, 3587–3592.

(26) Grabow, L.; Mavrikakis, M Mechanism of methanol synthesis on Cu through CO2 and CO hydrogenation. *Acs Catalysis* **2011**, *1*, 365–384.

(27) Liu, Y.-M.; Liu, J.-T.; Liu, S.-Z.; Li, J.; Gao, Z.-H.; Zuo, Z.-J.; Huang, W. Reaction mechanisms of methanol synthesis from CO/CO2 hydrogenation on Cu2O (111): comparison with Cu (111). *Journal of CO2 Utilization* **2017**, *20*, 59–65.

(28) Saussey, J; Lavalley, J. An in situ FT-IR study of adsorbed species on a Cu-ZnAl2O4 methanol catalyst under 1 MPa pressure and at 525 K: effect of the H2/CO/CO2 feed stream composition. *Journal of molecular catalysis* **1989**, *50*, 343–353.

(29) Studt, F.; Behrens, M.; Kunkes, E. L.; Thomas, N.; Zander, S.; Tarasov, A.; Schumann, J.; Frei, E.; Varley, J. B.; Abild-Pedersen, F., et al. The mechanism of CO and CO2 hydrogenation to methanol over Cu-based catalysts. *ChemCatChem* **2015**, *7*, 1105–1111.

(30) Rodŕíguez-Reinoso, F.; Sepúlveda-Escribano, A. Carbon as catalyst support. *Carbon materials for catalysis* **2008**, 131–155.

(31) Kukovecz, Á.; Kozma, G.; Kónya, Z. Multi-walled carbon nanotubes. *Springer handbook of nanomaterials* **2013**, 147–188.

(32) Miners, S. A.; Rance, G. A.; Khlobystov, A. N. Chemical reactions confined within carbon nanotubes. *Chemical Society Reviews* **2016**, *45*, 4727–4746.

(33) Pełech, I.; Narkiewicz, U.; Kaczmarek, A.; Jędrzejewska, A. Preparation and characterization of multi-walled carbon nanotubes grown on transition metal catalysts. *Polish Journal of Chemical Technology* **2014**, *16*, 117–122.

(34) King, C.; Ristroph, K. Nanotube & Carbon Fiber Overview, 2016.

(35) Dong, X.; Zhang, H.-B.; Lin, G.-D.; Yuan, Y.-Z.; Tsai, K. Highly active CNT-promoted Cu–ZnO–Al 2 O 3 catalyst for methanol synthesis from H 2/CO/CO 2. *Catalysis letters* **2003**, *85*, 237–246.

(36) Zhang, H.-B.; Dong, X.; Lin, G.-D.; Liang, X.-L.; Li, H.-Y. Carbon nanotube-promoted Co–Cu catalyst for highly efficient synthesis of higher alcohols from syngas. *Chemical communications* **2005**, 5094–5096.

(37) Zhang, Y.; Zhang, H.-B.; Lin, G.-D.; Chen, P.; Yuan, Y.-Z.; Tsai, K. Preparation, characterization and catalytic hydroformylation properties of carbon nanotubes-supported Rh–phosphine catalyst. *Applied Catalysis A: General* **1999**, *187*, 213–224.

(38) Wang, D.; Yang, G.; Ma, Q.; Wu, M.; Tan, Y.; Yoneyama, Y.; Tsubaki, N. Confinement effect of carbon nanotubes: copper nanoparticles filled carbon nanotubes for hydrogenation of methyl acetate. *Acs Catalysis* **2012**, *2*, 1958–1966.

(39) Chen, W.; Pan, X.; Bao, X. Tuning of redox properties of iron and iron oxides via encapsulation within carbon nanotubes. *Journal of the American Chemical Society* **2007**, *129*, 7421–7426.

(40) Zhang, Q.; Zuo, Y.-Z.; Han, M.-H.; Wang, J.-F.; Jin, Y.; Wei, F. Long carbon nanotubes intercrossed Cu/Zn/Al/Zr catalyst for CO/CO2 hydrogenation to methanol/dimethyl ether. *Catalysis today* **2010**, *150*, 55–60.

(41) Dong, X.; Shen, B.; Zhang, H.; Lin, G.; Yuan, Y. Study on Highly Active Catalysts and a Once-Through Process for Methanol Synthesis from Syngas. *Journal of Natural Gas Chemistry* **2003**, *12*, 49–55.

(42) Surisetty, V. R.; Tavasoli, A.; Dalai, A. Synthesis of higher alcohols from syngas over alkali promoted MoS2 catalysts supported on multi-walled carbon nanotubes. *Applied Catalysis A: General* **2009**, *365*, 243–251.

(43) Zao, H.; Liu, J.; Yan, B.; Yao, J.; Liu, S.; Chen, G. ZnO–ZrO2 coupling nitrogen-doped carbon nanotube bifunctional catalyst for co-production of diesel fuel and low carbon alcohol from syngas. *International Journal of Hydrogen Energy* **2024**, *63*, 460–471.

(44) Großmann, D.; Dreier, A.; Lehmann, C.; Grünert, W. Methanol synthesis over Cu–ZnO aggregates supported on carbon nanotubes. *Applied Catalysis A: General* **2015**, *504*, 351–360.

(45) Olivares, F.; Peón, F.; Henríquez, R.; del Río, R. S. Strategies for area-selective deposition of metal nanoparticles on carbon nanotubes and their applications: a review. *Journal of Materials Science* **2022**, 1–26.

(46) Dongil, A. B.; Pastor-Pérez, L.; Sepúlveda-Escribano, A.; García, R.; Escalona, N. Hydrodeoxygenation of guaiacol: Tuning the selectivity to cyclohexene by introducing Ni nanoparticles inside carbon nanotubes. *Fuel* **2016**, *172*, 65–69.

(47) Pan, X.; Bao, X. The effects of confinement inside carbon nanotubes on catalysis. *Accounts of chemical research* **2011**, *44*, 553–562.

(48) Qiang, F.; Gisela, W.; Su, D.-S. Selective filling of carbon nanotubes with metals by selective washing. *New carbon materials* **2008**, *23*, 17–20.

(49) Tessonnier, J.-P.; Ersen, O.; Weinberg, G.; Pham-Huu, C.; Su, D. S.; Schlogl, R. Selective deposition of metal nanoparticles inside or outside multiwalled carbon nanotubes. *ACS nano* **2009**, *3*, 2081–2089.

(50) Capobianchi, A.; Foglia, S.; Imperatori, P.; Notargiacomo, A.; Giammatteo, M.; Del Buono, T.; Palange, E. Controlled filling and external cleaning of multi-wall carbon nanotubes using a wet chemical method. *Carbon* **2007**, *45*, 2205–2208.

(51) Su, D. S.; Schlögl, R. Nanostructured carbon and carbon nanocomposites for electrochemical energy storage applications. *ChemSusChem: Chemistry & Sustainability Energy & Materials* **2010**, *3*, 136–168.

(52) Shahsavar, H.; Taghizadeh, M.; Kiadehi, A. D. Effects of catalyst preparation route and promoters (Ce and Zr) on catalytic activity of CuZn/CNTs catalysts for hydrogen production from methanol steam reforming. *International Journal of Hydrogen Energy* **2021**, *46*, 8906–8921.

(53) Solhy, A; Machado, B.; Beausoleil, J; Kihn, Y; Gonçalves, F; Pereira, M.; Órfão, J.; Figueiredo, J.; Faria, J.; Serp, P MWCNT activation and its influence on the catalytic performance of Pt/MWCNT catalysts for selective hydrogenation. *Carbon* **2008**, *46*, 1194–1207.

(54) Ros, T. G.; Van Dillen, A. J.; Geus, J. W.; Koningsberger, D. C. Surface oxidation of carbon nanofibres. *Chemistry–A European Journal* **2002**, *8*, 1151–1162.

(55) Małecka, B.; Łącz, A.; Drożdż, E.; Małecki, A. Thermal decomposition of d-metal nitrates supported on alumina. *Journal of Thermal Analysis and Calorimetry* **2015**, *119*, 1053–1061.

(56) Yuvaraj, S.; Fan-Yuan, L.; Tsong-Huei, C.; Chuin-Tih, Y. Thermal decomposition of metal nitrates in air and hydrogen environments. *The Journal of Physical Chemistry B* **2003**, *107*, 1044–1047.

(57) Mahajan, A.; Kingon, A.; Kukovecz, A.; Konya, Z.; Vilarinho, P. M. Studies on the thermal decomposition of multiwall carbon nanotubes under different atmospheres. *Materials Letters* **2013**, *90*, 165–168.

(58) Datsyuk, V.; Kalyva, M; Papagelis, K.; Parthenios, J.; Tasis, D; Siokou, A; Kallitsis, I; Galiotis, C. Chemical oxidation of multiwalled carbon nanotubes. *carbon* **2008**, *46*, 833–840.

(59) Jia, Z.; Wang, Z.; Liang, J.; Wei, B.; Wu, D. Production of short multi-walled carbon nanotubes. *Carbon* **1999**, *37*, 903–906.

(60) Rosca, I. D.; Watari, F.; Uo, M.; Akasaka, T. Oxidation of multiwalled carbon nanotubes by nitric acid. *Carbon* **2005**, *43*, 3124–3131.

(61) Dalebout, R.; Barberis, L.; Totarella, G.; Turner, S. J.; La Fontaine, C.; De Groot, F. M.; Carrier, X.; Van Der Eerden, A. M.; Meirer, F.; De Jongh, P. E. Insight into the Nature of the ZnO x Promoter during Methanol Synthesis. *ACS catalysis* **2022**, *12*, 6628–6639.

(62) Donoeva, B.; Masoud, N.; De Jongh, P. E. Carbon support surface effects in the gold-catalyzed oxidation of 5-hydroxymethylfurfural. *ACS catalysis* **2017**, *7*, 4581–4591.

(63) Arrigo, R.; Hävecker, M.; Wrabetz, S.; Blume, R.; Lerch, M.; McGregor, J.; Parrott, E. P.; Zeitler, J. A.; Gladden, L. F.; Knop-Gericke, A., et al. Tuning the acid/base properties of nanocarbons by functionalization via amination. *Journal of the American Chemical Society* **2010**, *132*, 9616–9630.

(64) Sun, Q.; Zhang, Y.-L.; Chen, H.-Y.; Deng, J.-F.; Wu, D.; Chen, S.-Y. A novel process for the preparation of cu/zno and cu/zno/al2o3ultrafine catalyst: Structure, surface properties, and activity for methanol synthesis from Co2+ h2. *Journal of Catalysis* **1997**, *167*, 92–105.

(65) Salmas, C.; Androutsopoulos, G. Mercury porosimetry: contact angle hysteresis of materials with controlled pore structure. *Journal of colloid and interface science* **2001**, *239*, 178–189.

(66) Donohue, M.; Aranovich, G. Adsorption hysteresis in porous solids. *Journal of colloid and interface science* **1998**, *205*, 121–130.

(67) Keluo, C.; Zhang, T.; Xiaohui, C.; Yingjie, H.; Liang, X. Model construction of micro-pores in shale: A case study of Silurian Longmaxi Formation shale in Dianqianbei area, SW China. *Petroleum Exploration and Development* **2018**, *45*, 412–421.

(68) Yu, H.; Jin, Y.; Peng, F.; Wang, H.; Yang, J. Kinetically controlled side-wall functionalization of carbon nanotubes by nitric acid oxidation. *The Journal of Physical Chemistry C* **2008**, *112*, 6758–6763.

(69) Ioannatos, G. E.; Verykios, X. E. H2 storage on single-and multi-walled carbon nanotubes. *International Journal of Hydrogen Energy* **2010**, *35*, 622–628.

(70) Fukumori, Y.; Nomura, T.; Adschiri, T.; Ohara, S.; Saito, F.; Naito, M.; Okuyama, K.; Kawahara, M.; Suzuki, H.; Sasaki, T., et al. In *Nanoparticle Technology Handbook*; Elsevier: 2008, pp 49–112.

(71) Wong, A.; Riojas, A. C.; Baena-Moncada, A. M.; Sotomayor, M. D. A new electrochemical platform based on carbon black paste electrode modified with α-cyclodextrin and hierarchical porous carbon used for the simultaneous determination of dipyrone and codeine. *Microchemical Journal* **2021**, *164*, 106032.

(72) Abdullah, M. P.; Zulkepli, S. A. In *AIP Conference Proceedings*, 2015; Vol. 1678.

(73) Osswald, S.; Havel, M.; Gogotsi, Y. Monitoring oxidation of multiwalled carbon nanotubes by Raman spectroscopy. *Journal of Raman Spectroscopy: An International Journal for Original Work in all Aspects of Raman Spectroscopy, Including Higher Order Processes, and also Brillouin and Rayleigh Scattering* **2007**, *38*, 728–736.

(74) Datye, A. K.; Xu, Q.; Kharas, K. C.; McCarty, J. M. Particle size distributions in heterogeneous catalysts: What do they tell us about the sintering mechanism? *Catalysis today* **2006**, *111*, 59–67.

(75) Jones, G.; Talley, S. K. The viscosity of aqueous solutions as a function of the concentration. *Journal of the American Chemical Society* **1933**, *55*, 624–642.

(76) Eskandari, S.; Tate, G.; Leaphart, N. R.; Regalbuto, J. R. Nanoparticle synthesis via electrostatic adsorption using incipient wetness impregnation. *ACS Catalysis* **2018**, *8*, 10383–10391.

(77) Ostgard, D.; Kustov, L; Poeppelmeier, K.; Sachtler, W. Comparison of Pt/KL catalysts prepared by ion exchange or incipient wetness impregnation. *Journal of Catalysis* **1992**, *133*, 342–357.

(78) Baatz, C; Decker, N; Prüße, U New innovative gold catalysts prepared by an improved incipient wetness method. *Journal of Catalysis* **2008**, *258*, 165–169.

(79) Zhu, X.; Cho, H.-r.; Pasupong, M.; Regalbuto, J. R. Charge-enhanced dry impregnation: A simple way to improve the preparation of supported metal catalysts. *Acs Catalysis* **2013**, *3*, 625–630.

(80) Delannoy, L.; El Hassan, N.; Musi, A.; Le To, N. N.; Krafft, J.-M.; Louis, C. Preparation of supported gold nanoparticles by a modified incipient wetness impregnation method. *The Journal of Physical Chemistry B* **2006**, *110*, 22471–22478.

(81) Şeker, B.; Dizaji, A. K.; Balci, V.; Uzun, A. MCM-41-supported tungstophosphoric acid as an acid function for dimethyl ether synthesis from CO2 hydrogenation. *Renewable Energy* **2021**, *171*, 47–57.

(82) Fan, X.; Jin, B.; Ren, S.; Li, S.; Yu, M.; Liang, X. Roles of interaction between components in CZZA/HZSM-5 catalyst for dimethyl ether synthesis via CO2 hydrogenation. *AIChE Journal* **2021**, *67*, e17353.

(83) Ren, S.; Shoemaker, W. R.; Wang, X.; Shang, Z.; Klinghoffer, N.; Li, S.; Yu, M.; He, X.; White, T. A.; Liang, X. Highly active and selective Cu-ZnO based catalyst for methanol and dimethyl ether synthesis via CO2 hydrogenation. *Fuel* **2019**, *239*, 1125–1133.

(84) Kundakovic, L.; Flytzani-Stephanopoulos, M Reduction characteristics of copper oxide in cerium and zirconium oxide systems. *Applied Catalysis A: General* **1998**, *171*, 13–29.

(85) Panagiotopoulou, P; Christodoulakis, A; Kondarides, D.; Boghosian, S Particle size effects on the reducibility of titanium dioxide and its relation to the water–gas shift activity of Pt/TiO2 catalysts. *Journal of Catalysis* **2006**, *240*, 114–125.

(86) Zhang, Y.; Sun, Q.; Deng, J.; Wu, D.; Chen, S. A high activity Cu/ZnO/Al2O3 catalyst for methanol synthesis: Preparation and catalytic properties. *Applied Catalysis A: General* **1997**, *158*, 105–120.

(87) Bartholomew, C. H. Mechanisms of catalyst deactivation. *Applied Catalysis A: General* **2001**, *212*, 17–60.

(88) Voorhees, P. W. The theory of Ostwald ripening. *Journal of Statistical Physics* **1985**, *38*, 231–252.

(89) Dalebout, R.; Visser, N. L.; Pompe, C. L.; de Jong, K. P.; de Jongh, P. E. Interplay between carbon dioxide enrichment and zinc oxide promotion of copper catalysts in methanol synthesis. *Journal of catalysis* **2020**, *392*, 150–158.

9 Appendix

Table 7: Reactor Tube Loadings

Block	Reactor	Catalyst I.D.	Wt%		Grain size catalyst (X-Y µm)	Weighed mass sample (mg)	Weighed mass SiC diluent (mg)	Height sample + SiC (cm)	Height post-bed SiC (cm)
			Cu	Zn					
B1	**1**	Mw	0	0	75-150	60.08	180.20	10.5	2.3
	2	Ox	0	0	75-150	60.17	180.68	6.9	2.3
	3	1E18	18	7	75-150	60.04	180.07	6.7	2.6
	4	1E7	7.2	2.8	75-150	60.01	180.51	7.1	2.5
B2	**5**	1I7	7.2	2.8	75-150	60.15	180.87	7.2	2.5
	6	1O7c	7.2	2.8	75-150	60.05	180.04	7.2	2.3
	7	1O7	7.2	2.8	75-150	60.55	180.51	6.9	2.6
	8	Ox	0	0	75-150	30.20	180.19	5.8	2.5
B3	**9**	1E7	7.2	2.8	75-150	30.96	180.68	5.6	2.5
	10	CZA			75-150	15.81	179.96	4.6	2.5
	11	Blank	0	0	0	0	0	2.9	2.9
	12	SiC blank	0	0	75-150	0	180.34	4.5	2.5
B4	**13**	1E18	18	7	75-150	30.5	180.60	5.3	2.4
	14	1I7	7.2	2.8	75-150	30.3	180.53	5.3	2.3
	15	1O7c	7.2	2.8	75-150	30.2	180.01	5.5	2.5
	16	1O7	7.2	2.8	75-150	30.2	180.34	5.4	2.3

Table 8: Pore structures of pristine and loaded MWCNTs

Sample	Pore (nm)	Total area (m^2/g)	Total pv (cm^3/g)	Micropore area (m^2/g)	Mesopore area (m^2/g)	Micropore volume (cm^3/g)	Mesopore volume (cm^3/g)
Mw	1.95	197	1.02	37.42	160	0.018	0.911
Ox	2.08	225	0.83	16.92	209	0.009	0.736
1E18	2.07	150	0.72	7.57	142	0.003	0.695
1E7	2.03	169	0.83	17.69	151	0.009	0.756
1I18	2.10	224	0.71	31.02	193	0.015	0.694
1I7	2.12	241	1.02	7.14	234	0.002	0.929
1I7c	2.07	244	0.88	21.86	222	0.010	0.761
1O7	2.05	195	0.74	14.29	181	0.007	0.690
2E14	2.00	162	0.56	28.47	134	0.013	0.550
2E18	2.06	157	0.53	22.44	135	0.011	0.515

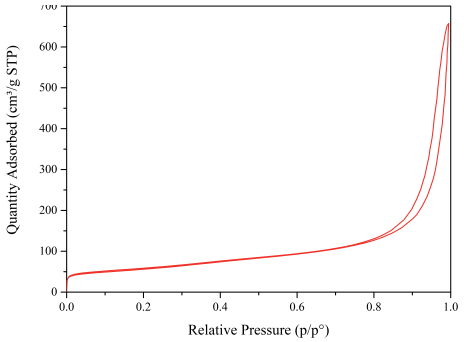

(a) Mw

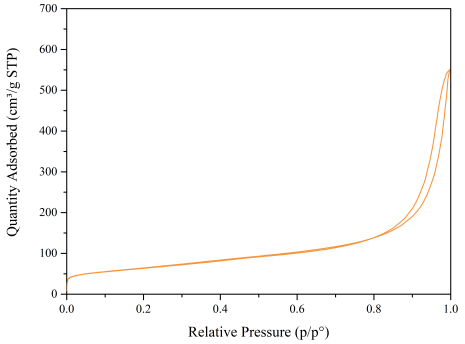

(b) Ox

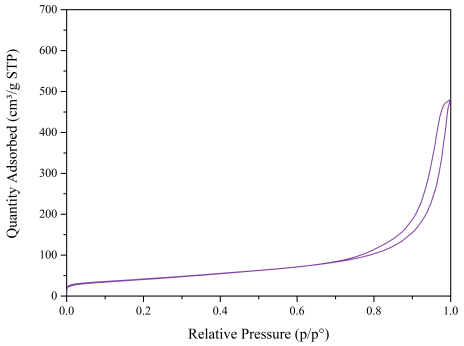

(c) 1E18

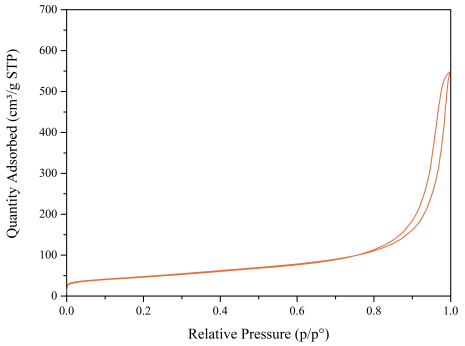

(d) 1E7

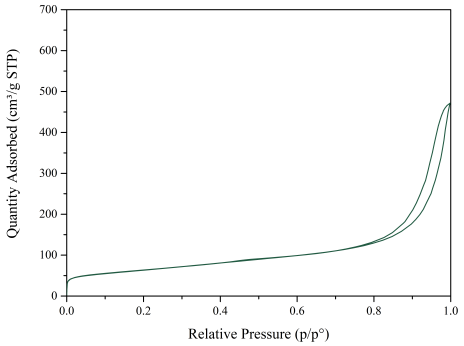

(e) 1I18

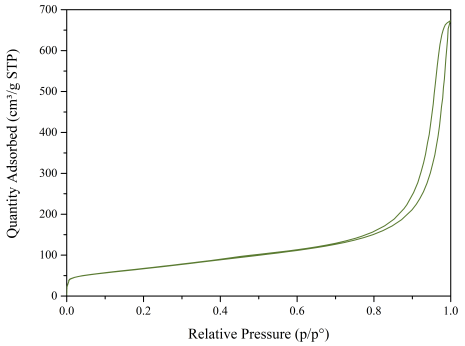

(f) 1I7

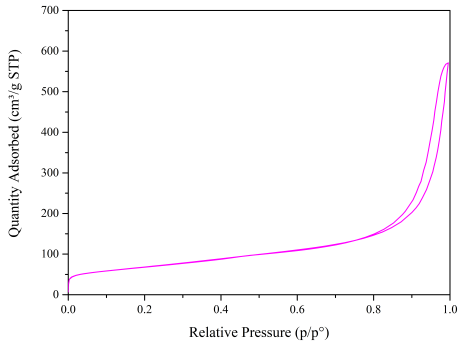

(g) 1I7c

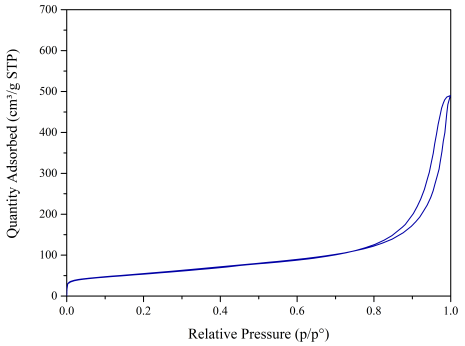

(h) 1O7

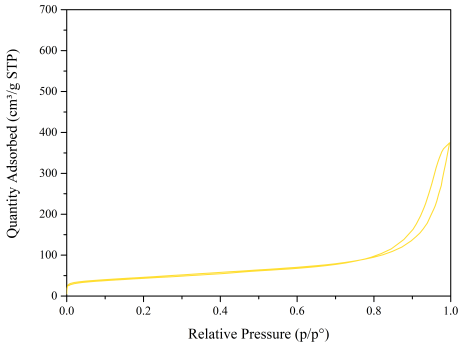

(i) 2E14

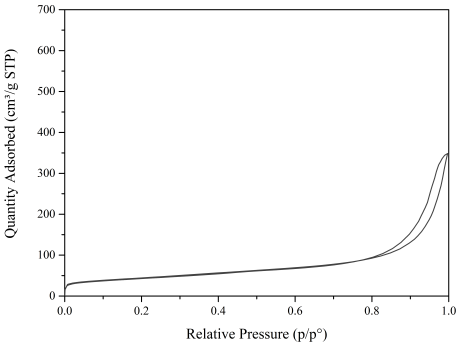

(j) 2E18

Figure 25: Physisorption plot plots for the different prepared supports

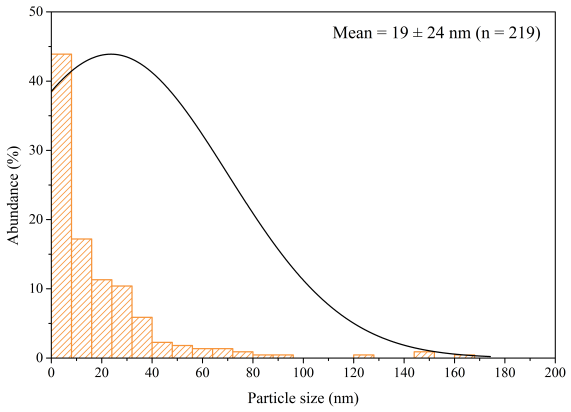

(a) Particle size distribution of 1E18

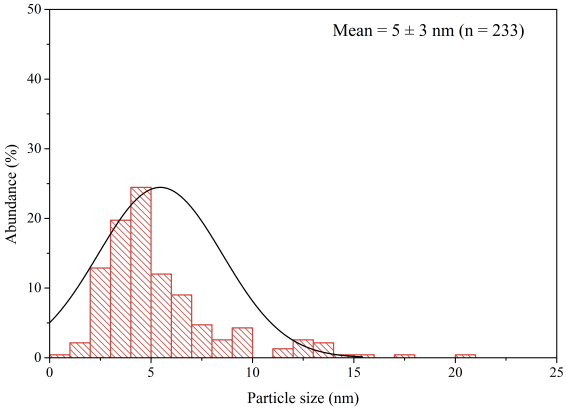

(b) Particle size distribution of 1E7

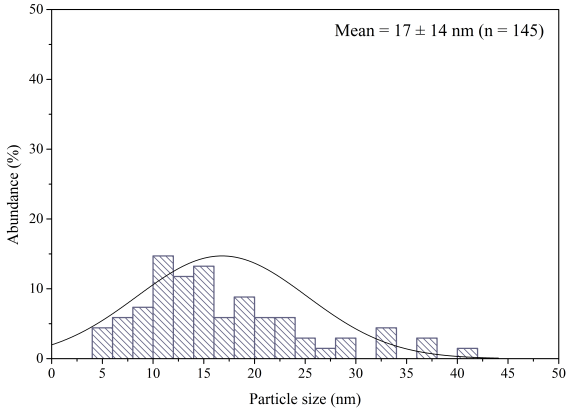

(c) Particle size distribution of 1I18

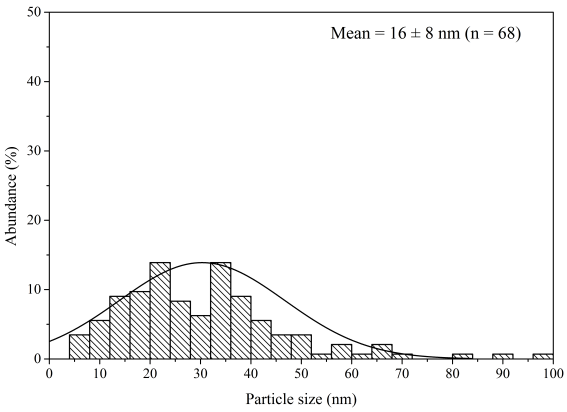

(d) Particle size distribution of 1I7

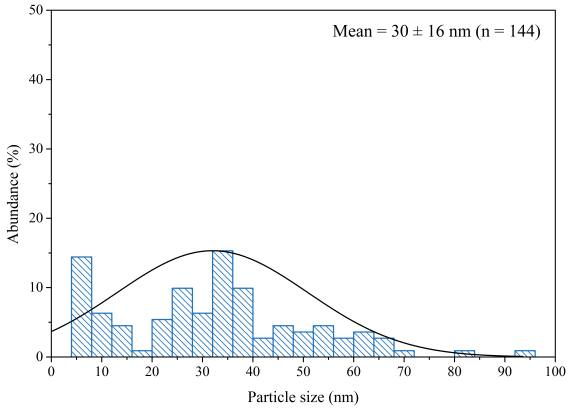

(e) Particle size distribution of 1I7c

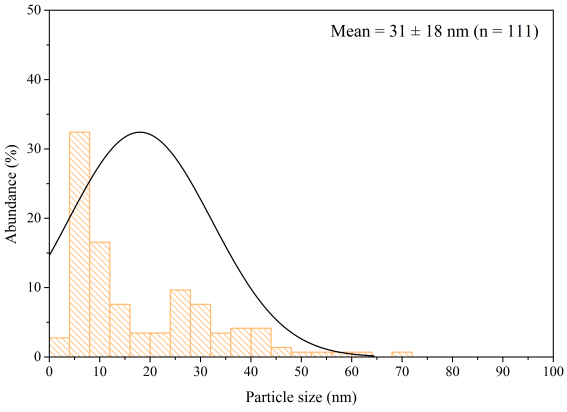

(f) Particle size distribution of 1O7

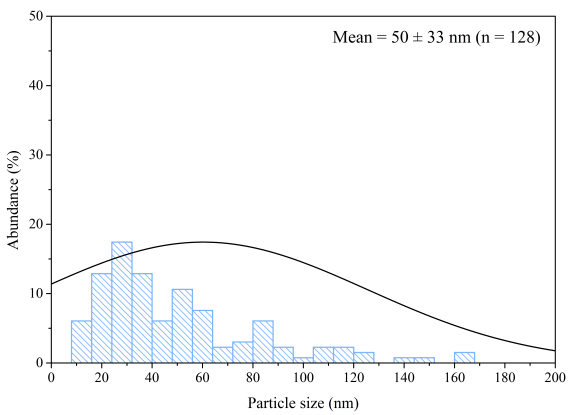

(g) Particle size distribution of 2E14

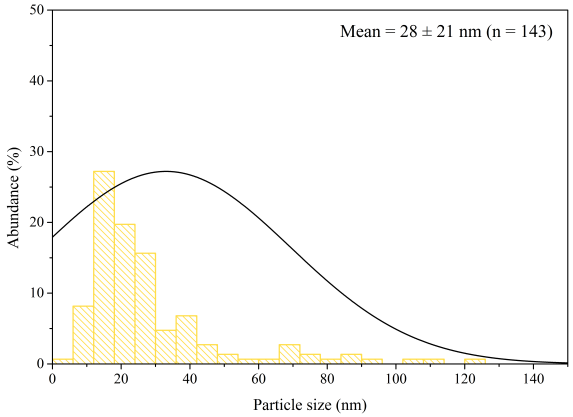

(h) Particle size distribution of 2E18

Figure 26: Particle size distributions for the different prepared supports

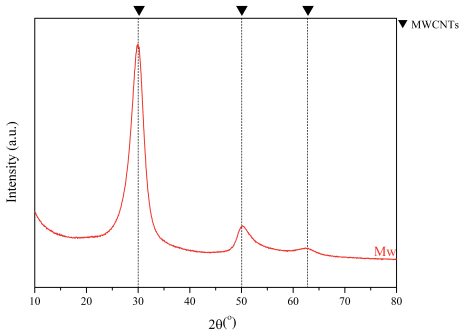

(a) XRD of Mw

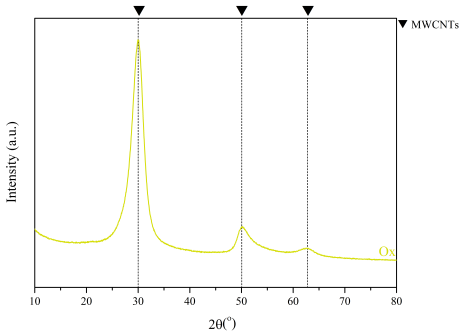

(b) XRD of Ox

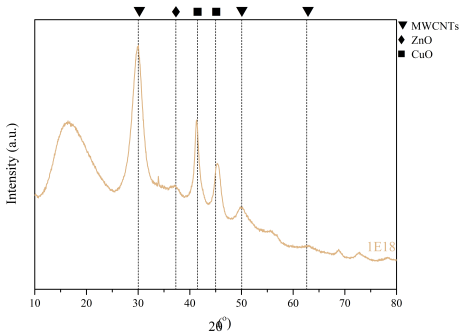

(c) XRD of 1E18

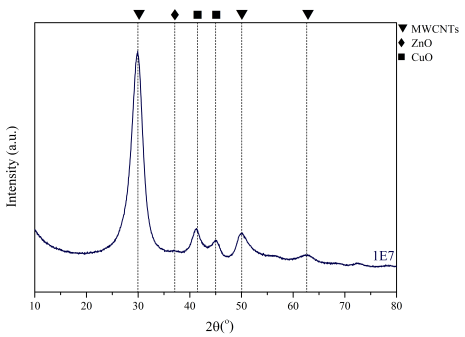

(d) XRD of 1E7

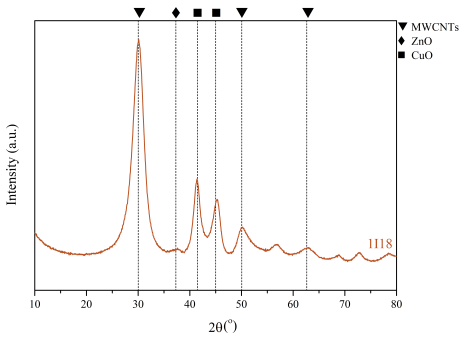

(e) XRD of 1I18

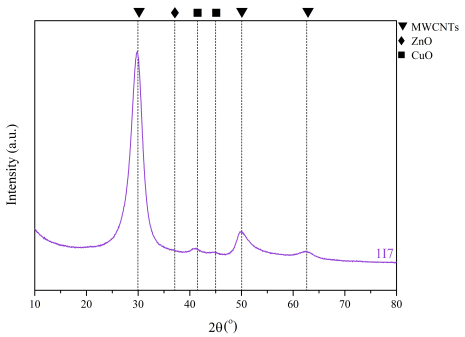

(f) XRD of 1I7

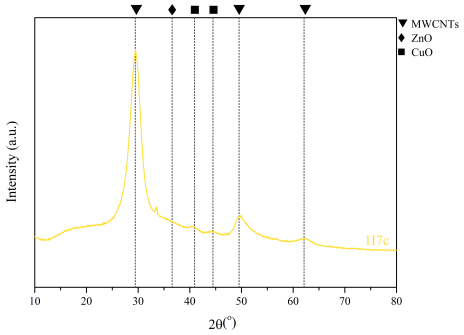

(g) XRD of 1I7c

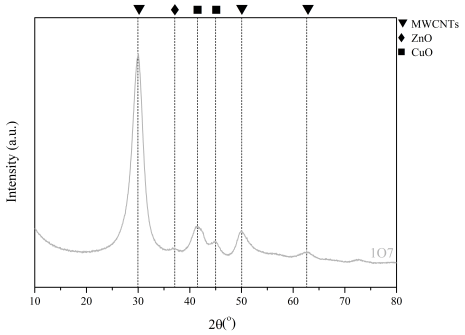

(h) XRD of 1O7

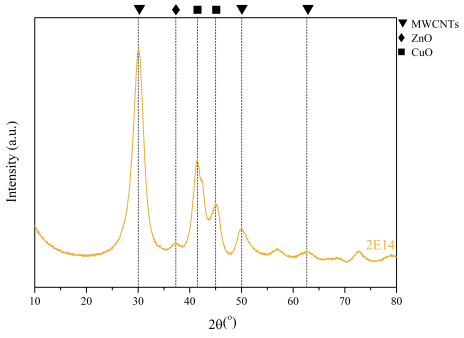

(i) XRD of 2E14

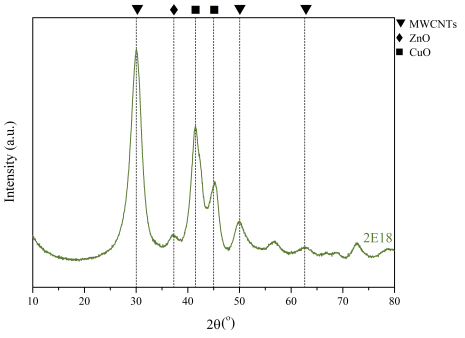

(j) XRD of 2E18

Figure 27: XRD plots for the different prepared supports